COLLEGE OF ENGINEERING

VIRGINIA POLYTECHNIC INSTITUTE AND STATE UNIVERSITY

BLACKSBURG, VIRGINIA

College of Engineering
Virginia Polytechnic Institute & State University
Blacksburg, Virginia 24061

VPI-E-82-4 March 1982

ADVANCES IN MOIRE INTERFEROMETRY FOR THERMAL RESPONSE OF COMPOSITES

Ernest W. Brooks, Jr.[1]
Carl T. Herakovich[2]
Daniel Post[2]
Michael W. Hyer[3]

Department of Engineering Science & Mechanics

Interim Report 27
The NASA-Virginia Tech Composites Program

NASA Cooperative Agreement NCC1-15

Prepared for: Environmental Effects Branch
National Aeronautics & Space Administration
Langley Research Center
Hampton, VA 23665

[1]Graduate student now with David Taylor Naval Ship Research and Development Center

[2]Professor of Engineering Science & Mechanics

[3]Associate Professor of Engineering Science & Mechanics

BIBLIOGRAPHIC DATA SHEET	1. Report No. VPI-E-82-4	2.	3. Recipient's Accession No.

4. Title and Subtitle

ADVANCES IN MOIRÉ INTERFEROMETRY FOR THERMAL RESPONSE OF COMPOSITES

5. Report Date March 1982

6.

7. Author(s)

E. W. Brooks, Jr., C. T. Herakovich, D. Post, M. W. Hyer

8. Performing Organization Rept. No. VPI-E-82-4

9. Performing Organization Name and Address

Virginia Polytechnic Institute & State University
Engineering Science & Mechanics
Blacksburg, Virginia 24061

10. Project/Task/Work Unit No.

11. Contract/Grant No.

CA NCC1-15

12. Sponsoring Organization Name and Address

National Aeronautics & Space Administration
Langley Research Center
Hampton, Virginia 23665

13. Type of Report & Period Covered

14.

15. Supplementary Notes

16. Abstracts

An experimental technique for precise measurement of the thermal response of both sides of a laminated composite coupon specimen is presented. The technique uses Moiré interferometry with fringe multiplication which yields a sensitivity of 833 nm (32.8 μin.) per fringe. The reference gratings used in this technique are virtual gratings and are formed by partially mirrorized glass prisms in close proximity to the specimen. Results are compared with both results obtained from tests which used Moiré interferometry on one side of composite laminates, and with those predicted by classical lamination theory.

The technique is shown to be capable of producing the sensitivity and accuracy necessary to measure a wide range of thermal responses and to detect small side to side variations in the measured response.

Tests were conducted on four laminate configurations--[0], [90], $[0/\pm45/90]_s$, $[0/90/\pm45]_s$--of T300/5208 graphite epoxy over a temperature range of 297K (75°F) to 422K (300°F). The technique presented allows for the generation of reference gratings for temperature regimes well outside that used in these tests.

17. Key Words and Document Analysis. 17a. Descriptors

composites, Moiré interferometry, thermal response, graphite-epoxy

17b. Identifiers/Open-Ended Terms

17c. COSATI Field/Group

18. Availability Statement

Distribution Unlimited

19. Security Class (This Report) UNCLASSIFIED

21. No. of Pages 67

20. Security Class (This Page UNCLASSIFIED

22. Price

ACKNOWLEDGEMENTS

This work was supported by the Environmental Effects Branch, NASA Langley Research Center. Thanks are due to Dr. Darrel R. Tenney, Branch Head, Dr. Stephen S. Tompkins, and Mr. David E. Bowles for their many helpful suggestions and encouragements during the course of this investigation. Thanks are also due to Ms. Catherine Barnett, Ms. Charlene Christie, and Ms. Vanessa McCoy for typing the manuscript.

TABLE OF CONTENTS

List of Tables

LIST OF FIGURES

1. INTRODUCTION

In the field of modern structural materials great interest exists in the use of fiber reinforced composites. The ability to control basic material properties by varying constituents in the composite lamina and to design combinations of laminae into laminates which give very specific structural response creates nearly unlimited advanced structural design possibilities. However, for fine tuned designs, very accurate measurements of the responses of these laminates to various types of loading are necessary if the design is to be truly optimal. One such response which must be accurately measured is that due to thermal loading. The coefficient of thermal expansion (CTE) for typical laminates in use today ranges from -1 $\mu\varepsilon$/ K (-.5 $\mu\varepsilon/^0F$) to 30 $\mu\varepsilon$/ K (17 $\mu\varepsilon/^0F$) and there is great interest in laminates or composite structures, such as space antennas, with "near zero" thermal expansion in some direction. The method used to determine these coefficients must therefore be very accurate and cover a broad range of responses.

A survey of existing methods for measuring thermal strains in low expansion materials is presented by Wolff [1] and includes discussions of the resistance strain gage, an optical-mechanical lever-type device, Fizeau and Michelson interferometers, and holographic speckle interferometry. Due to problems with limited accuracy, specimen geometries, or requirements of sophisticated and expensive optical

equipment for these methods, another method was sought for the thermal expansion testing of composite laminates.

Recently, Bowles, et al. [2,3] introduced Moiré interferometry for thermal expansion measurements of composite laminates. Advantages of the method presented are:

1. purely geometric measurement technique;
2. displacement sensitivity of 833 nm (33 μin) per fringe
3. resolution of 7 με ;
4. influence of specimen end effects eliminated;
5. full field observations permitting measurement of displacements along specimen boundaries;
6. technique is relatively easy to implement and is inexpensive.

This report presents the following extensions to the technique developed by Bowles, et al.:

1. use of a prism to provide a virtual reference grating, thereby eliminating the temperature limit (480 K) (400° F) of the diffraction grating used by Bowles;
2. simultaneous measurement of displacements on both sides of the test specimen, which provides the necessary data for separating longitudinal strains from bending strains.

In the present work the prism is used as an alternate method of generating a reference grating for testing over the same temperature range used in Bowles [2]. However, since the prism can generate a reference grating at much higher temperatures than the diffraction grating

used by Bowles, its use here is a first step in developing a 620 K (650° F) temperature capability for this method. Use of two-sided viewing is important. Even though the composite laminates tested here have nominally systemetric configurations, there are numerous sources of non-symmetrical response. For example: a $[0/\pm45/90]_S$ laminate, 1.11 mm (43.7 mils) thick, which is missing 0.035 mm (1.4 mils) of the outside layer on one side, will experience, over a temperature range of 125 K (225° F), a bending strain of approximately 25% its true longitudinal strain; microcracking damage in composite laminates as reported in [4,5,6] can result in antisymmetrical or localized behavior; and small variations in ply orientation can be a source of bending strains.

The method presented in this report provides a means of determining the extensional strains in composite laminates due to thermal loading to an accuracy of ±3.5 $\mu\varepsilon$. Results are presented for tests on two unidirectional Gr/E laminates - [0], [90]- and two quasi-isotropic Gr/E laminates - $[0/\pm45/90]_S$ and $[0/90/\pm45]_S$. Comparison of test results with theoretical values based on laminate analysis are presented, as well as comparison with the results obtained by Bowles [3]. These comparisons indicate good results, and some modificiations are suggested which should further improve the results obtainable with this method.

2. MOIRÉ INTERFEROMETRY

2.1 General Theory

The theory of Moiré interferometry has been presented by a number of authors, with detailed presentations being given by Guild [7], Chiang [8] and Post [9]. The salient features of this theory pertinent to the method of testing developed in this report are presented below.

Moiré interferometry begins with a plane wavefront of coherent light. This wavefront is split into two plane wavefronts by either a diffraction grating, which produces a real reference grating, or by some combination of mirrors or prisms, which produces a virtual reference grating. In either case the reference grating is comprised of only two wavefronts, or two dominant wavefronts in terms of intensity, which interfere with each other and form an interference pattern with pitch g_r given by

$$g_r = \frac{\lambda}{2 \sin \alpha} \tag{2.1}$$

where λ is the wavelength of light being used, and 2α is the included angle between the two wavefronts. A further requirement is that the two wavefronts be oriented symmetrically with respect to the normal to the specimen grating, as shown in Fig. 1. This symmetry condition was shown by Post [10] to remove any effect of out-of-plane deformations on the Moiré patterns. The two wavefronts comprising the reference grating are

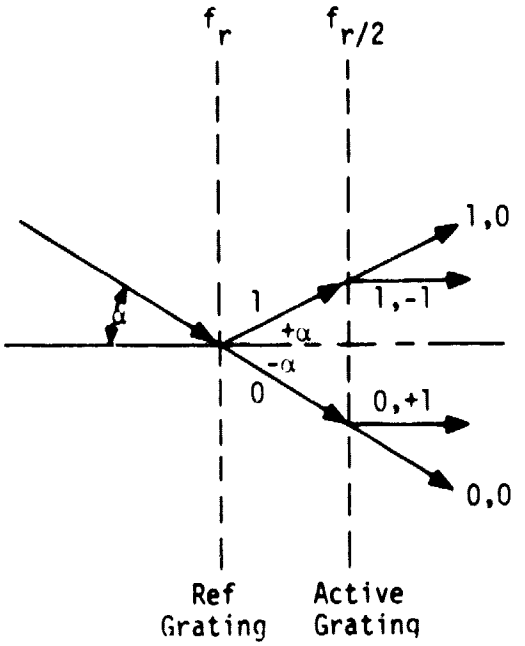

Fig. 1 Reference & Active Gratings - Symmetric Double Order Dominance

then incident upon an active grating attached to the test specimen as shown in Fig. 1.

In his work on Moiré fringe multiplication, Post [10] has shown that for reference grating with pitch g_r, as defined in Eqn. (2.1), and active grating with pitch g_a such that,

$$g_a = \beta g_r \tag{2.2}$$

where β is an integer value, the sensitivity of a test using these gratings is strictly a function of g_r and is independent of g_a. Furthermore, if β is an even integer, and both the planes and grating lines of the reference grating and active grating are approximately parallel, then the diffraction rays of the order $+\beta/2$ and $-\beta/2$ emerge from the active grating parallel with the normal to the grating, forming a two beam interference pattern known as Moiré fringes. Equation (2.2) can be rewritten in terms of the frequencies of the reference and active gratings, f_r and f_a,

$$f_r = \beta f_a \tag{2.3}$$

where:

$$f = 1/g \tag{2.4}$$

For the situation described by Eqn. (2.3) the $+\beta/2$ and $-\beta/2$ orders are parallel, and the interference pattern is a null field containing zero Moiré fringes of extension. If the relationship between active and ref-

erence grating was slightly altered from that given in Eqn. (2.3) to

$$f_r = \beta(f_a \pm \delta) \text{ where } \delta << f_a \tag{2.5}$$

then diffraction orders $+\beta/2$ and $-\beta/2$ would be inclined to one another and would produce an interference pattern with a frequency of $\beta\delta$ Moiré fringes. If the specimen is extended or contracted f_a decreases or increases, which causes a change in the frequency of observed Moiré fringes. A change of one fringe corresponds to a displacement of g_r. The strain associated with changes in Moiré fringes over some gage length L is given by

$$\varepsilon_m = \frac{(N - N_i) \cdot g_r}{L} \tag{2.6}$$

where N_i is the initial number of Moiré fringes over L and N is the number of Moiré fringes over L after deformation.

An important consequence of Eqn. (2.6) is that if there is some warpage of the reference wavefront due to an imperfect optical setup, it will be present to the same extent in each fringe pattern and will be subtacted out by the $N-N_i$ term. Another consequence of Eqn. (2.6), which relates to fringe ordering, is that since N and N_i are the number of fringes occuring over length L, rather than the number of the fringes themselves, the fringe orders assigned to a pattern are relative values rather than absolute.

2.2 Literature Review

A very thorough review of the literature concerning both thermal expansion of composites as well as the use of Moiré interferometry can be found in Bowles, et al. [3]. Several papers concerning use of Moiré interferometry are mentioned here to supplement that list. Papers by Walker and McKelvie [11] and Rowlands and Vallem [12] discuss casting replicas of active Moiré grids and interogating these castings later in the laboratory. These methods are valuable for taking measuremnts in non-laboratory settings and when loadings are other than environmental. For CTE measurements desired here these methods are not practical and real time observation and recording of the Moiré pattern is used. In another paper of note, Post and Baracat [13] describe the use of a virtual reference grating in Moiré interferometry to measure displacements in an off-axis composite under uniaxial loading. The optical setup used to create the virtual reference grating in that work could not be used directly in a thermal expansion test as the divided beams would have to travel relatively long paths in the thermal environment before being recombined and the thermal currents encountered would cause movements in the fringes, resulting in unclear or disappearing fringe patterns. However, since commercially available diffraction gratings have a temperature limit of about 500 K (440° F), and since some of the laminates ultimately to be tested with the method presented in this report will require a test temperature of 620 K (650° F), a technique

for use of a virtual reference grating in a thermal expansion test was developed.

2.3 Virtual Reference Grating by Prism

2.3.1 Generating the Reference Grating

As mentioned earlier, the reference grating in Moiré interferometry, regardless of how it is generated, is nothing more than the interference pattern produced by two plane wavefronts of coherent light. These wavefronts are inclined to the normal to the active grating at angles $+\alpha$ and $-\alpha$ as shown in Fig. 1, with the pattern having a specified pitch, g_r, as in Eqn. (2.1). Figure 2 shows the ray diagram for a reference grating created using a prism with semi-transparent mirror surfaces. The interference angle, α, is given by

$$\sin \alpha = \frac{f_r \lambda}{2} \tag{2.7}$$

where f_r is the desired reference grating frequency and λ the wavelength of the coherent light being used. The prism angle, θ, is given by

$$\sin \theta = \frac{1}{n} \sin \alpha \tag{2.8}$$

where n is the index of refraction of the prism. Finally the angle of the incoming ray to the normal to the reference grating, ϕ is given by

$$\sin(\phi + \theta) = n \sin(2\theta) \tag{2.9}$$

When these relations are satisfied the following steps produce the de-

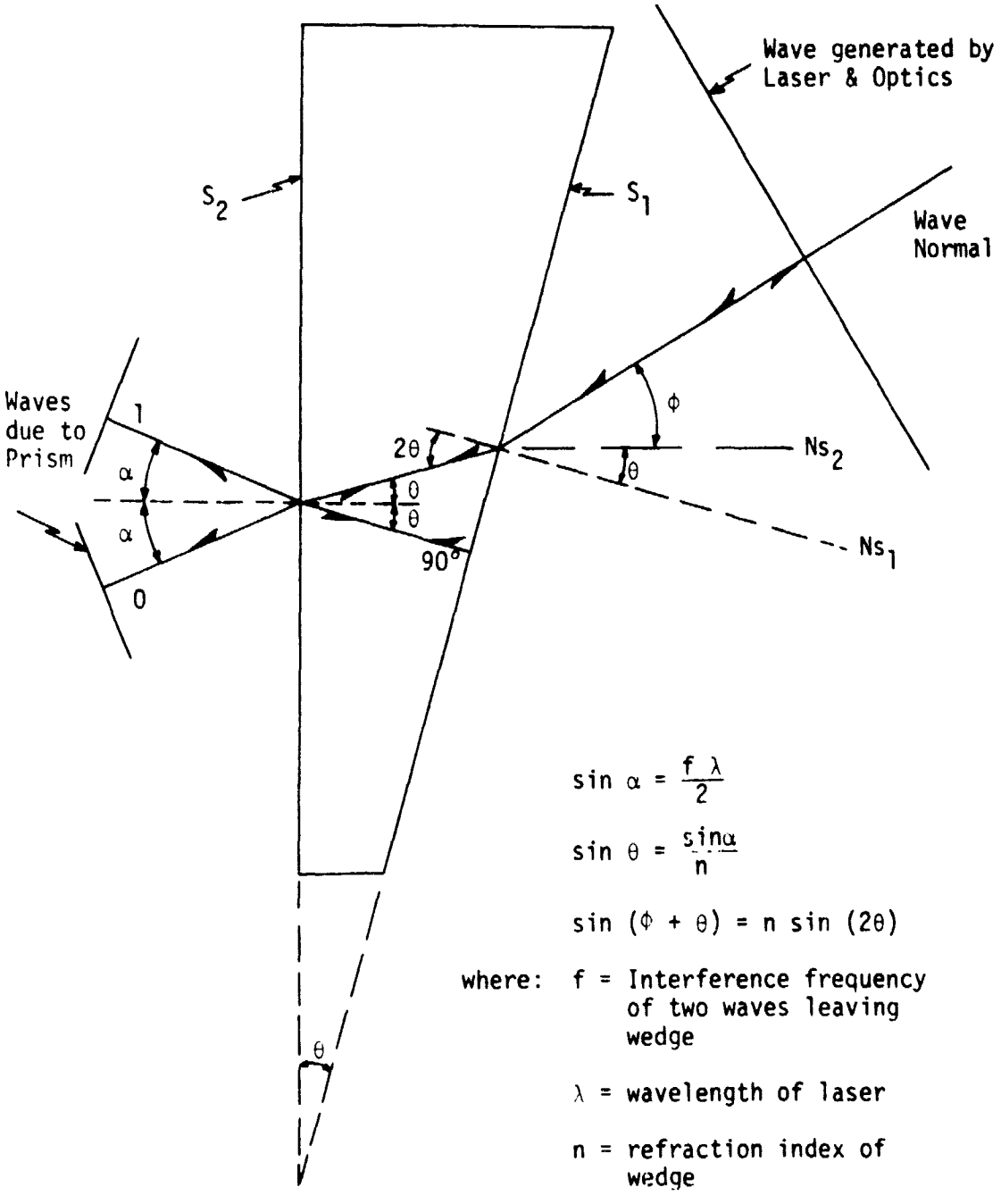

Fig. 2 Two-Beam Interference By Mirrorized Prism

sired reference grating:

1. the incoming ray is partially transmitted upon reaching surface 1 (S_1) of the prism, with the transmitted ray being refracted to an angle of 2θ to the normal to S_1;
2. this ray then strikes surface 2 (S_2) of the prism where it is partially transmitted and partially reflected. The transmitted portion is again refracted and corresponds to the "0"th diffraction order of a diffraction grating with frequency f_r.
3. the reflected ray is normal to S_1 where it is returned to S_2 along the same path it traveled to S_1. Upon reaching S_2 it is partially transmitted and partially reflected. The transmitted portion is refracted and corresponds to the 1st diffraction order of a diffraction grating with frequency f_r.
4. the reflected portion of this ray ultimately returns to the source of the original ray of light and thus provides a means of accurate alignment of the system just described.

Since the initial wavefront of light is divided and recombined within the prism, and since the prism can be placed as close as desired to the active grating on the specimen, the problems discussed earlier associated with existing methods of generating virtual gratings in a thermal test environment are eliminated.

2.3.2 Extraneous Rays

A problem with extraneous rays from diffraction orders other than the two desired, similar in effect to that reported by Bowles, et al. [3], was anticipated but never encountered. As shown in Fig. 3 both reference grating beams produce "0" diffraction orders after incidence upon the active grating. These two "0" orders are partially reflected upon reaching the back of the prism, and when the reflected beams reach the active grating, additional ±1 diffraction orders are produced. To eliminate the possibility of interference patterns associated with these follow-up diffractions being mixed with the patterns from the initial diffractions, or additional patterns being generated by interference of the additional orders with the initial orders, a means of isolating pairs of diffraction orders was provided. An adjusting screw shown in Fig. 3 allowed the rotation of the specimen relative to the reference grating. A small rotation of this type would cause a much larger separation of the additional pairs from the original pair. An aperture plate could then be positioned to allow only the original pair of rays to proceed to the camera. However, due to the additional partial reflections, transmissions, and additional diffraction sequence, these extraneous rays were of such low intensity that they could never be seen on the aperture plate and hence did not produce fringes of sufficient intensity or contrast to be visible in the recorded Moiré patterns, even if not blocked by the aperture plate.

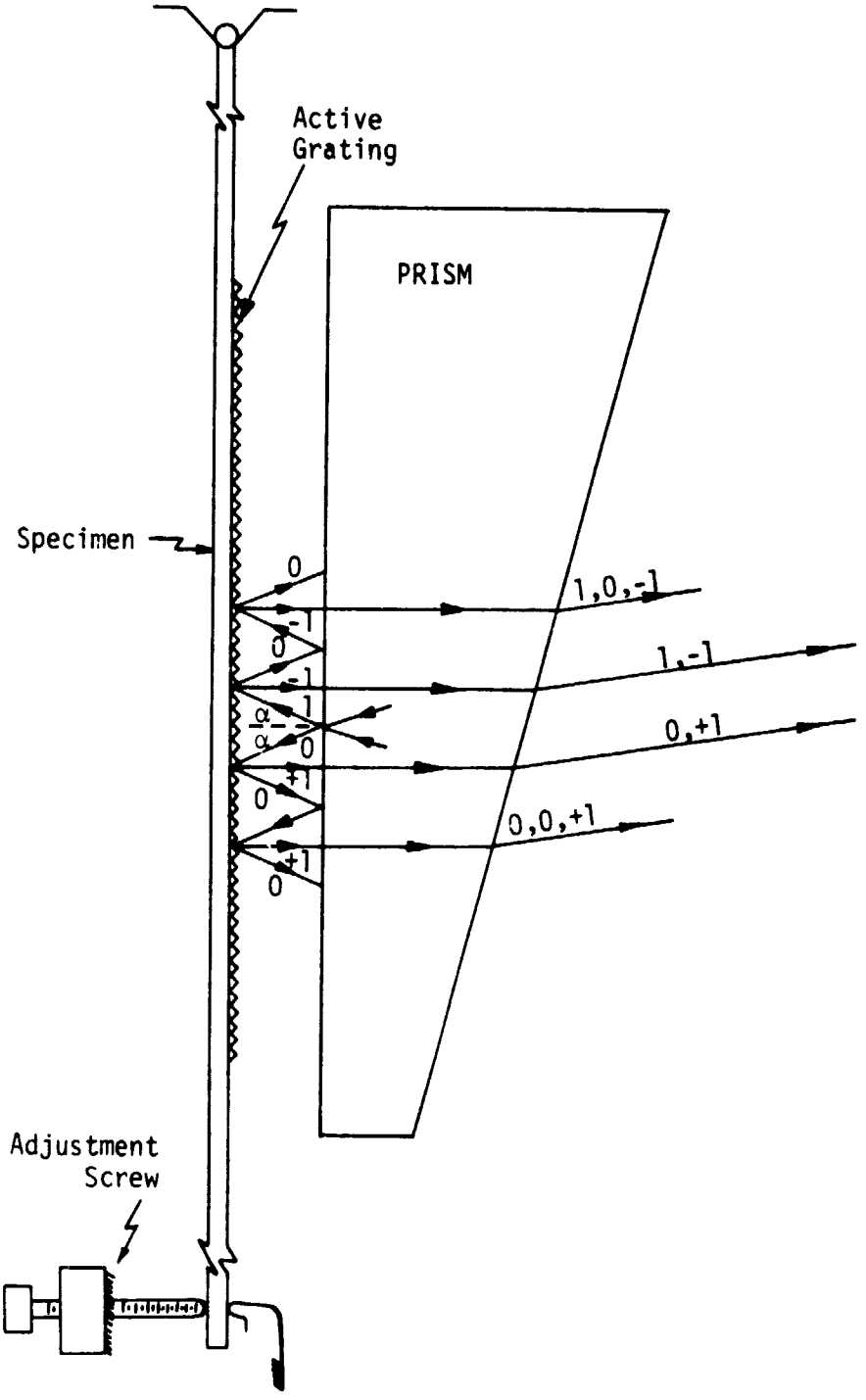

Fig. 3 Extraneous Diffraction Orders

3. EXPERIMENTAL PROCEDURE

3.1 Two Sided Replication and Grating Mold - Specimen Alignment

In order to collect Moiré data on both faces of the specimen simultaneously, a phase-type grating was replicated on each face. The gratings formed on the specimen are silicone rubber cast in place against a mold with a corrugated surface of approximately 600 ℓ/mm (15,250 ℓ/in.). The corrugated surface was formed on a high resolution photographic plate - either Kodak HRP-1A or 120-02. The method used to make the molds and replicate them is detailed in Refs. [3], [9] and [13]. (For best results the two gratings were replicated at the same time, thereby avoiding any damage to the grating on one face while replicating on the other.)

Accurate alignment of the mold on the specimen was achieved by using the fixture shown schematically in Fig. 4. The photoplate to be used as the diffraction grating mold is attached to the rotating base through the photoplate holder. A laser beam is directed at the mold and the mold is rotated until the diffraction rays line up on the knife edge, which is parallel to the fixed base of the fixture. A piece of tool steel flat stock (1/32" x 1/2" x 2") with its long edge in contact with the fixed base is then bonded to one side of the mold's corrugated surface. The long edge of the flat stock can be attached at less than 0.1° off the normal to the grating corrugations. The inside edge of the flat stock is then butted against the edge of the specimen during replication to yield precise alignment of active grating on the specimen. As

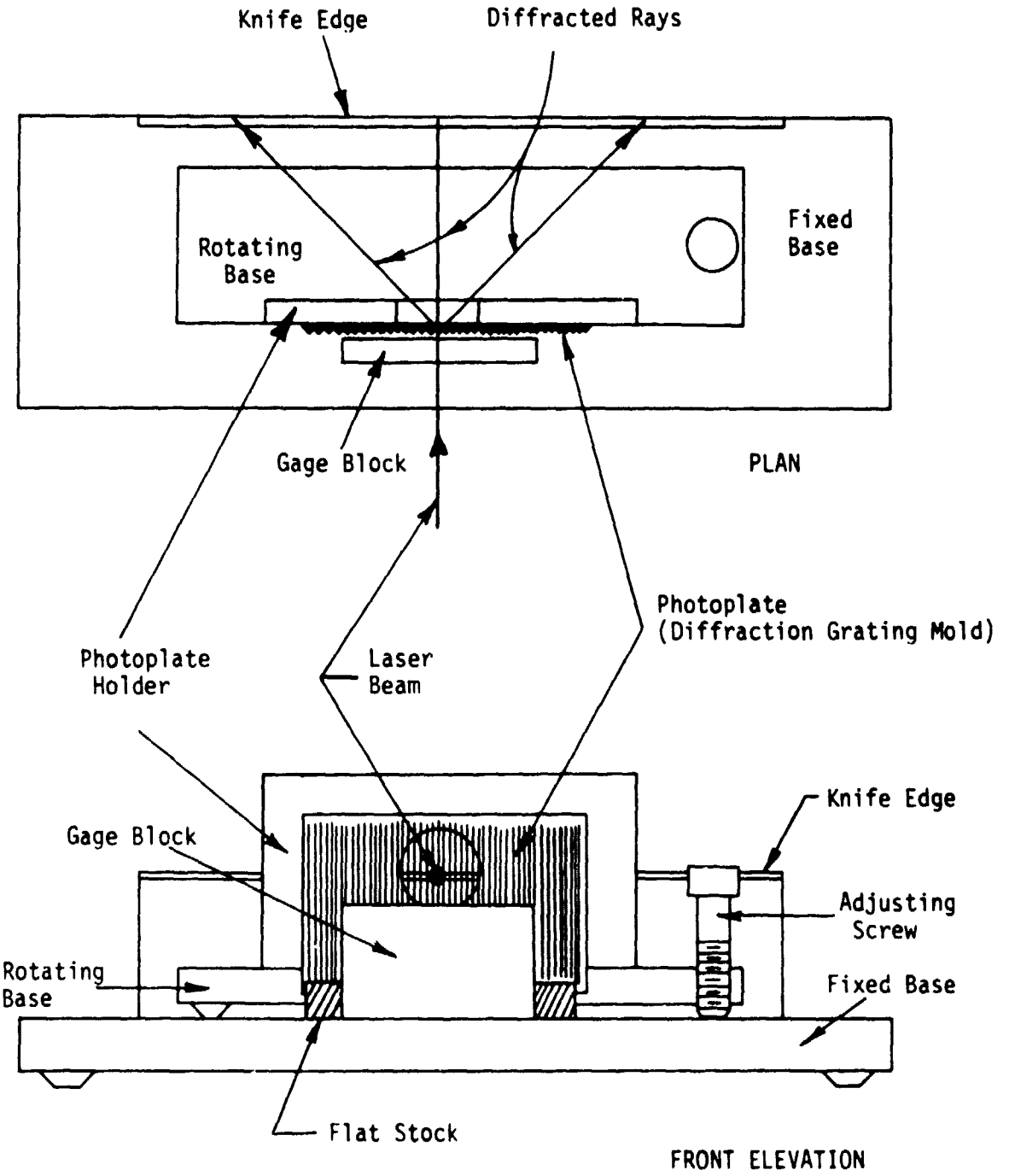

Fig. 4 Fixture for Aligning Longitudinal Gage Line on Mold & Mold on Specimen

noted by Bowles [3] this is especially important in reducing any effect of the shearing CTE in the unidirectional specimens.

In addition to aiding in the alignment of the piece of flat stock, the same fixture was used to align the longitudinal and horizontal gage lines on the mold. A razor was used to scribe the gage lines in the photoplate's emulsion. The longitudinal gage line was scribed using a gage block placed on the fixed base in front of the mold (as shown in Fig. 4) as a guide. The horizontal gage lines were scribed using the same gage block rotated 90° as a guide, and a series of gage blocks with appropriate thicknesses to set the desired spacing between lines. This aids in reducing the error associated with the longitudinal gage line not being perpendicular to the specimen grating lines described by Bowles, et al. [2]. With this increased accuracy, errors associated with rigid body rotation are reduced to approximately ±1 $\mu\varepsilon$.

3.2 Experimental Apparatus

3.2.1 Inside the Test Oven

After diffraction gratings were replicated on both faces of the specimen, a thin steel rod, 1.6 mm (1/16") x 50 mm (2"), was attached to one end of the specimen with the same silicone rubber as was used for the gratings. The steel rod supported the suspended specimen when it was placed in the test fixture, Fig. 5. Figures 3 and 5 also show a screw for out of plane rotation about the supporting rod. This

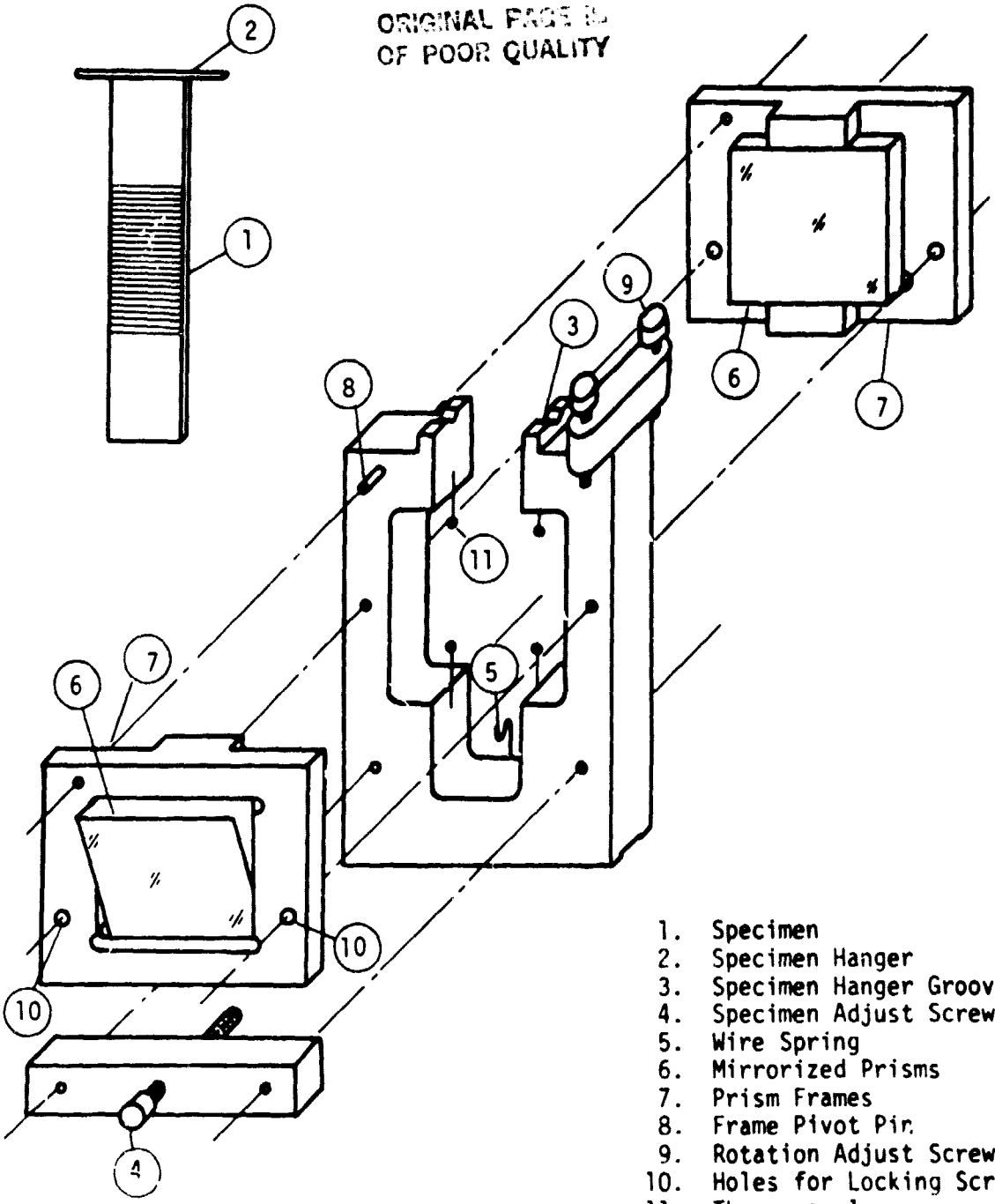

Fig. 5 Wedge & Specimen Fixtures

rotational adjustment was provided for the reasons discussed in Section 2.3.2.

Also attached to the specimen support are the two prisms and their support frames, as shown in Fig. 5. The prisms were fastened in the frames using silicone rubber adhesive. The frames were then attached to the specimen supporting fixtures in such a way as to allow in-plane rotation for alignment of the reference grating with the specimen grating. Micrometer adjusting screws provided sensitive in-plane rotation adjustment to achieve the desired degree of alignment.

The specimen and prism support was mounted on a pedestal arrangement attached to the base of the overall setup. The pedestal arrangement was comprised of a steel pedestal attached to the base, which entered the test oven through a hole in the floor. A block of pyrex glass was placed between this steel pedestal and the specimen support fixture so as not to provide a continuous metal path through which heat could flow. The steel pedestal was wrapped with fiberglass insulation to reduce heat loss through the metal and the hole through which it was inserted. Figure 6 shows the entire assemblage inside the oven. The laboratory oven (ATS Series 2911) was capable of maintaining test temperatures in the range of 88 to 700 K (-300 to 800° F) and had a viewing window in the front and a window in each side for illumination of the gratings and observation of the fringes.

Figure 7 shows the location of the 4 Type J, iron-constantin thermocouples used to measure temperature during testing. These thermo-

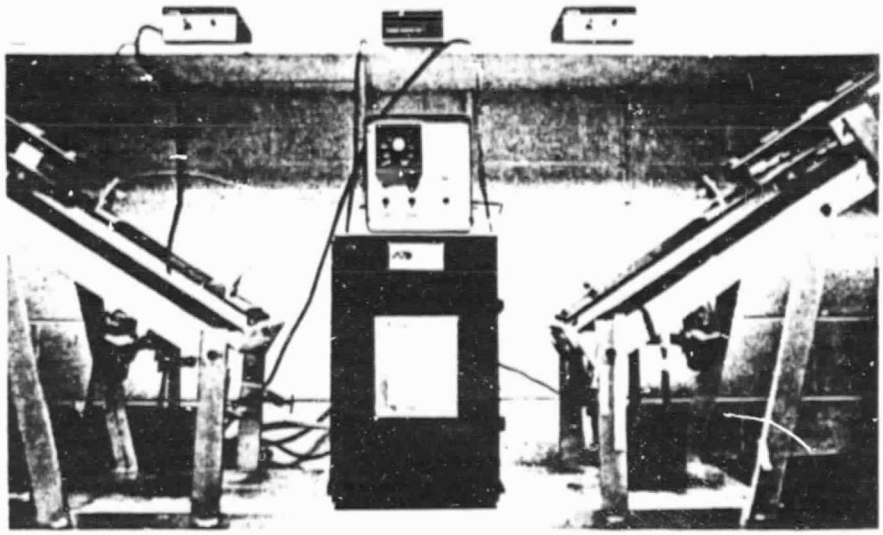

OVERALL TEST SETUP

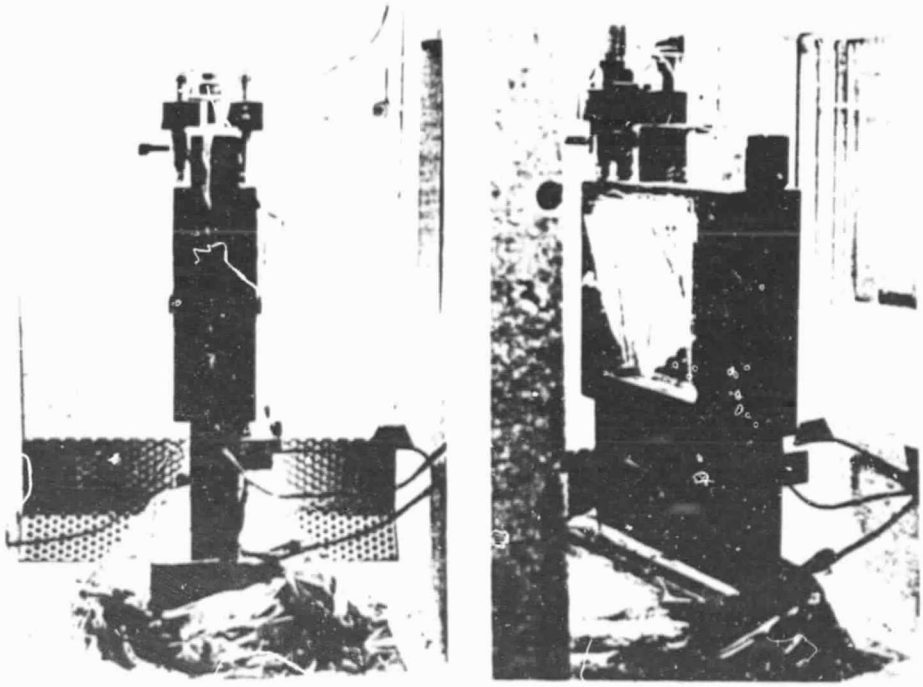

SPECIMEN & PRISM HOLDER

Fig. 6 Test Apparatus

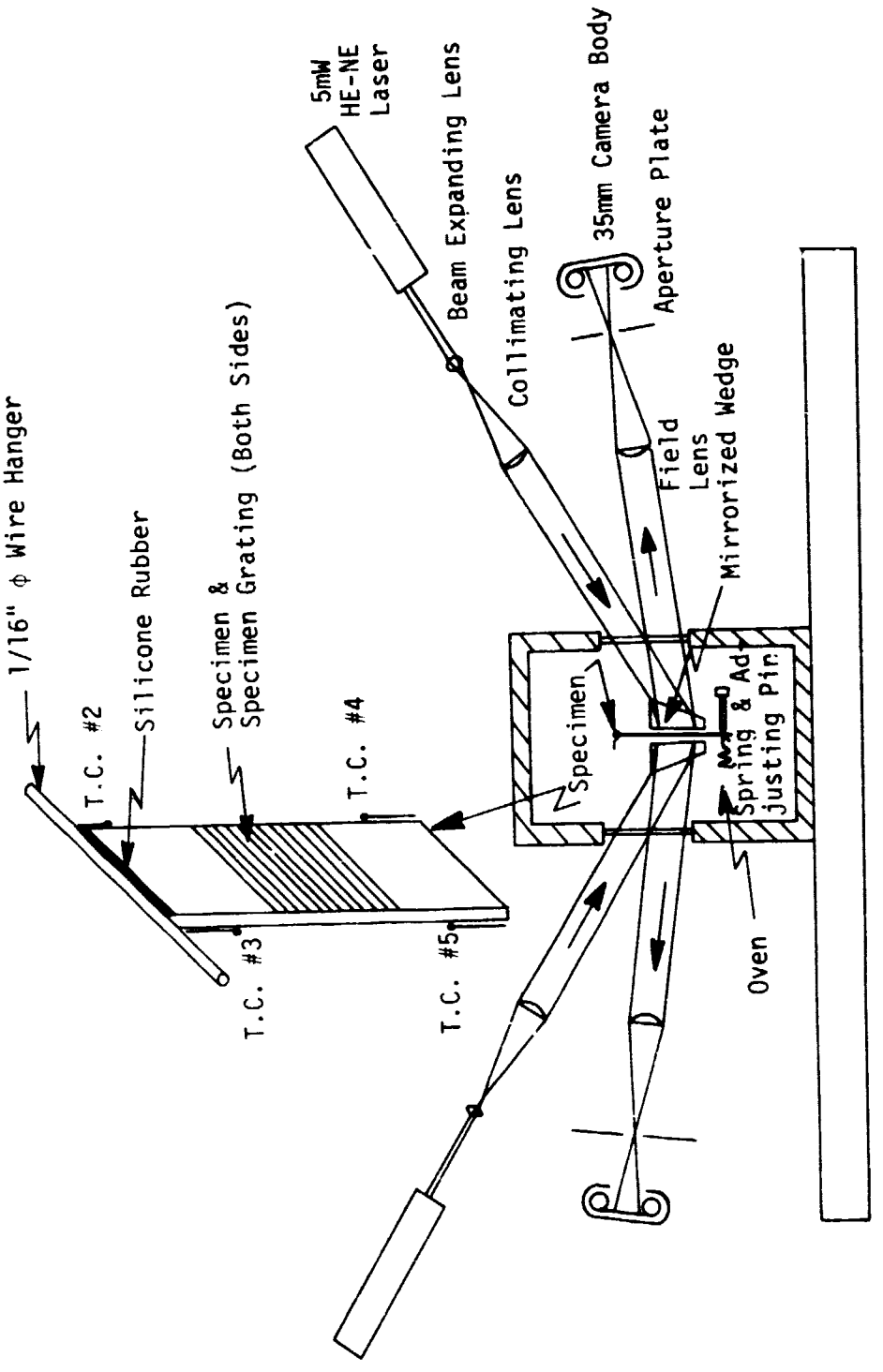

Fig. 7 Test Stand

couples are positioned immediately adjacent to the test specimen but do not contact it. With the long temperature soak times employed (1- 1 1/2 hrs.) the air temperature around the specimen should be the same as that of the specimen. Temperatures were monitored with a Doric Trendicator which gave readouts to 0.1° F.

3.2.2 Optical Setup

Figure 6 contains a photograph of the overall experimental setup and Fig. 7 gives a schematic representation of the same, with an identification of the elements. The support structure is aluminum except the piece to which the laser, beam expander and collimating lens are attached, which is steel. A 5 mw He-Ne laser was used. The collimating and decollimating lenses are ordinary plano-convex lenses. The support structure is set approximately at the proper angle of incidence and adjustments in both the vertical and horizontal planes are provided. Fringe patterns are recorded on 35 mm Kodak Techical Pan (2415) Film, which has the desirable features of high contrast capabilities, extended red panchromatic sensitivity, and dyed gel backing which suppresses curl as well as halation.

3.2.3 Prism Description

The prisms used in this work were cut from a Corning Fused Silica No. 7940 blank with a room temperature index of refraction, n, of 1.4571 for the wavelength of light used. The overall dimensions were 63 mm tall, 55 mm wide, and 6 mm thick at the narrow base (2.5" x 2.2" x

0.25"). Surface flatness was specified to be within 1/10 wavelength, and multi-layer dielectric coatings were applied for approximately 60% reflectance and 40% transmittance. The room temperature frequency of the prisms was found to be 1198.4 ℓ/mm (30,440 ℓ/in) by viewing the Moiré pattern produced by a 600 ℓ/mm Bausch and Lomb diffraction grating and the prisms.

One problem discovered after testing began was the relatively large amount of strain derived from the Moiré data which was attributable to changes occurring in the reference grating during testing compared with the small strains actually occuring in the specimen grating (see Section 3.4). These apparent strains attributable to the prism occur because of a relatively large change of n with temperature (dn/dT) of approximately 10×10^{-6}/K (5.6×10^{-6}/° F). Prisms for follow-up testing with this method will be made from an optical glass designated LaK N 12-678552 which has a dn/dT of approximately -0.2×10^{-6}/K (-0.1×10^{-6}/° F). This smaller dn/dT will yield smaller reference grating corrections to be applied to the Moiré results which in general, should lead to more accurate results.

3.3 Specimen Description

As mentioned earlier graphite-epoxy laminates were tested in this research. The specific material system was T300/5208 with the specimens being cut from the same panels as those tested by Bowles [3]. For comparison with results obtained in that work the same four laminate con

figurations were tested - [0], [90], $[0/\pm45/90]_s$ and $[0/90/\pm45]_s$. The specimens were machined to a length of 127.0 mm (5 in) and width of 25.4 mm (1 in). Each laminate had eight plies, with thicknesses, after surface preparation, of 1.02 mm (0.040 in) for the unidirectional specimens and 1.07 mm (0.042 in) for the quasi-isotropic specimens.

The surface preparation involved the removal of the weave pattern left on the surface after laminate fabrication. Removal was necessary as the pattern caused an unacceptable reduction of image quality in the Moiré patterns. Light sanding with a 600 grit silicon carbide paper was found to sufficiently remove this pattern while preserving the necessary degree of specimen thickness uniformity. The unidirectional laminates had one smooth side and therefore needed sanding only on one side, while the quasi-isotropic laminates had to be sanded on both sides. Approximately 0.025 mm (0.001 in) of material was removed from each side requiring sanding.

All specimens were dried for three weeks prior to testing. The specimens were dried at 340 K (152° F). The oven used did not have an enforced dry atmosphere, and the atmosphere at 340 K was in the 5-10% relative humidity range. This limitation apparently left some residual moisture in the laminates and caused changes in moisture in the laminate during testing. Total weight loss during the drying period was approximately 0.4% for the unidirectional laminates and 0.5% for the quasi-isotropic laminates.

3.4 Data Collection and Reduction

3.4.1 Collection

The procedure for conducting tests on the laminates was to first photograph the fringe patterns at temperature intervals of approximately 25 K (45° F) from room temperature (295 K (70° F)) up to 435 K (325° F), and back down to room temperature. Due to the existence of some vibration from the test oven and its blurring effect on the fringe pattern, the oven was shut off during the photographing of the fringe pattern. Even though it took only a few seconds for the vibration to damp out and exposures to be made, the thermocouples were read before and after making the exposure and temperaures were averaged. The thermocouple readings differed by 0.5 to 1.0 °F. In general 1-1 1/2 hours were needed between setting a new temperature and stabilization of the 4 thermostat readouts. An additional 30 min. soak time after stabilization insured temperature equilibrium of the specimen. The thermal cycle was repeated to provide more data if needed. Exposure times of 1 second with the Kodak Technical Pan film were generally adequate. Figure 8 shows typical fringe patterns at several temperatures. In addition to the fringe patterns, Fig. 8 also illustrates the longitudinal and horizontal gage lines which were scribed on the grating mold as described in Section 3.1 and transferred to the specimen during replication. The longitudinal gage line is perpendicular to the grating lines and is in the direction along which strains were to be detemined. Only the central line was used in this

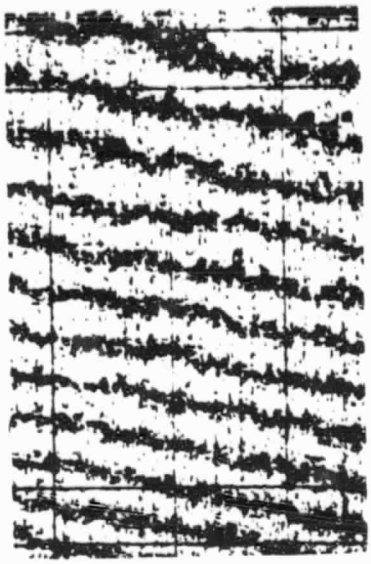

300°K (78°F)

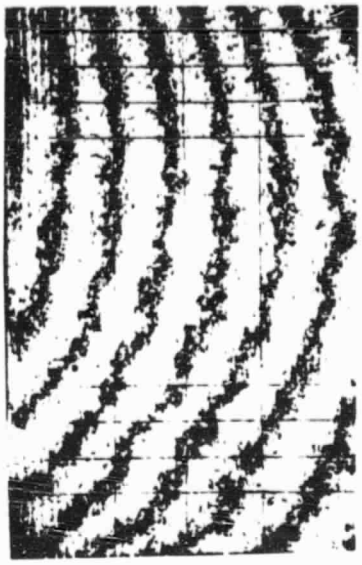

355°K (180°F)

382°K (228°F)

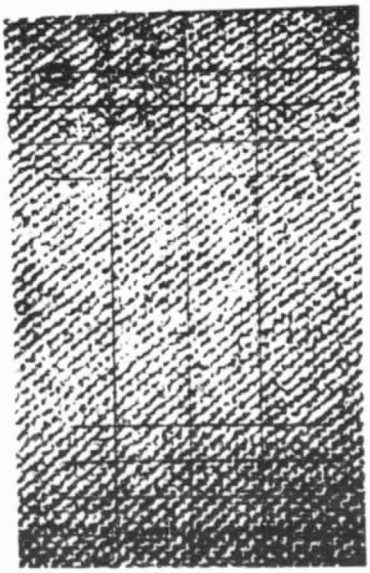

435°K (324°F)

Fig. 8 Typical Fringe Patterns

analysis. The horizontal gage lines are parallel to the grating lines and their position along the longitudinal gage line was determined to the nearest 2.5 mm (0.0001 in). One of the extreme horizontal gage lines was marked to determine the "0"th gage line for measurement purposes.

As was mentioned at the close of Section 2.1, fringe orders are assigned in a relative rather than an absolute sense. For convenience, the fringe nearest the "0"th horizontal gage line lying outside the test section was assigned the "0"th order. The succeeding fringes are numbered sequentially through the test section. The sign of the fringe order is determined as indicated in Section 3.4.2.

After assigning initial fringe orders, fractional fringe values were measured at each horizontal gage mark position with the aid of a photographic enlarger, which was used to project each fringe pattern negative on to a white background with a magnification of approximately 10X. This magnification made it possible to estimate each fringe order at a gage mark to 0.1 fringe.

3.4.2 Fringe Order Sign Convention

In order to solve Eqn. (2.6) in a consistent manner and to derive a functional relationship between the apparent strain obtained from the Moiré data, ε_m, the specimen strain, ε_s, and the reference grating strain, ε_r, a convention for determining the sign of N is needed. In this work this convention is:

$$N = (f_r - \beta f_s) \cdot L \tag{3.1}$$

where f_r is the frequency of the reference grating and f_s is the frequency of the specimen (active) grating. The terms on the right hand side cannot be stated explicitly for any temperature in the test range, but if the sign of the initial (room temperature) value of N is determined the sign of subsequent values of N may be determined by observation. Noting initial values with the subscript i, Eqn. 3.1 is rewritten

$$N_i = (f_{r_i} - \beta f_{s_i}) \cdot L \tag{3.1b}$$

To determine the sign of N_i use is made of the setup depicted in Fig. 3. The active grating is rotated about an axis parallel with its grating lines by use of the adjustment screw, until either a maximum or minimum number of fringes appear. At this point the active grating and the virtual reference grating produced by the prism are parallel and the number of fringes repesent the difference between f_{r_i} and βf_{s_i}. Since rotating the active grating from a position not parallel with that of the reference grating to a position which is parallel with it always causes a reduction in apparent frequency of the active grating (ultimately to its actual value) then, if the fringe pattern observed was a maximum, f_{r_i} is greater than βf_{s_i} and if the pattern was a minimum, f_{r_i} is less than βf_{s_i}. Having thus determined the larger of the two values f_{r_i} and βf_{s_i} the sign of N_i is set according to the

convention represented by Eqn. (3.1b). The signs of subsequent values of N are easily determined by noting whether N increases or decreases with increasing temperature: if N increases the sign is the same as N_i, if it decreases the sign is the same as N_i until a zero value is reached, after which the sign is opposite that of N_i for continued increase in temperature.

3.4.3 Moiré Data Reduction

As Eqn. (2.6) states, the information to be taken from the photographs of fringe patterns will be used to determine the change in the number of fringes over a known length, occurring during some temperature change. The factor $(N-N_i)/L$ can be computed simply by finding the number of fringes between two gage marks at an initial temperature, doing the same at some other temperature, subtracting the two numbers and dividing the result by the distance between the two gage marks. A problem with this is that it provides no check on the precision or correctness of the readings of fringe values or gage mark positions. Recognizing that the term $(N-N_i)/L$ is equivalent to the slope of the curve represented by the change in relative fringe order at positions along the longitudinal gage line versus the relative distance to those positions, a convenient and more statistically precise method is used to generate this term from the Moiré data. In this method, the fringe values at each horizontal gage mark on the initial temperature pattern are subtracted from the fringe values at the same gage mark on subsequent temp-

erature patterns. For each temperature, these differences and the relative position of the gage marks to which they correspond form the set of data pairs to which a first order (assumed uniform strain field) least squares curve fit is made, the slope of this curve being equivalent to the term $(N-N_i)/L$.

The horizontal gage marks are grouped as shown in Fig. 8 as a compromise between two objectives - for a least squares slope the points used have an increasing influence the closer they are to the end points of the data; and data points should be spread out along the specimen length to avoid dependence on one area where a material defect may cause locally erroneous results or a fringe order may be difficult to measure.

To compare the use of this gage line arrangement with that used by Bowles, et al., a comparison of the standard deviation of the slopes for the two cases is made. The standard deviation of the slope of a first order least squares fit is:

$$S_m = S_y \sqrt{\frac{n}{n\Sigma x_i^2 - (\Sigma x_i)^2}} \qquad (3.2)$$

where n is the number of (x,y) pairs, x is the independent variable considered to be relatively free of error; and S_y is the standard deviation of the dependent variable, y. Even though the number of readings obtained from either gage line arrangement of a particular temperature does not constitute a truly statistically significant set of data, it can be assumed that the standard deviation of the $(N - N_i)$ values - S_y -

would be the same for either test since it is primarily a measure of how well the fringe orders may be read. The comparison is then that of the term under the radical in Eqn. (3.2), which involves the positional values of the gage lines - the independent variable. For the gage lines used by Bowles, i.e. a gage length of 33 mm (1.3 in.) with 14 gage lines evenly spaced along the entire length Eqn. (3.6) yields:

$$S_m = 2.61 \times 10^{-2} \cdot S_{\Delta N}(\ell/mm) \qquad (3.2a)$$

In these tests the gage line arrangement is the same as that by Bowles, with the six gage lines in the middle region eliminated. For this arrangement Eqn. (3.2) yields

$$S_m = 2.72 \times 10^{-2} \cdot S_{\Delta N}\ (\ell/mm) \qquad (3.2b)$$

This indicates the accuracy obtainable with the gage line arrangement used here to be 96% of that obtainable with the arrangement in Bowles while using 43% fewer data points.

For the case where a fringe order is read only at each end of a 33 mm gage length the expected slope deviation would be

$$S_m = 4.29 \times 10^{-2} \cdot S_{\Delta N}(\ell/mm) \qquad (3.2c)$$

3.4.4 Prism Calibration

In order to reduce the information obtained from fringe patterns generated by the test specimens into specimen strains, the contribution of the prism had to be established. To do this a test was run using a specimen of known thermal response. In [3] Bowles used Fizeau

Interferometry tc determine the thermal response of Corning ULE$_{TM}$ (Ultra Low Expansion) titanium silicate code 7971. This ULE material was subsequently used as a test specimen to calibrate the prisms. This specimen could not be supported in the same manner as the composite test specimens were, but it was fitted into one of the wedge-holding frames so that the active grating (600 ℓ/mm) on its surface was in the same proximity to the prism in the other holder as one face of a composite specimen would be. From the fringe patterns generated in this test, a Moiré strain, ε_m, is computed as noted in the previous section.

Using this ε_m and the strain from the 3rd order polynomial derived by Bowles from the ULE's ε vs. T response as the specimen strain, ε_s, the strain, ε_r, attributable to the prism is determined at each data point using the relationship developed in the next section. These ε_r values, along with the temperature at which they occur, form the data pairs for a least squares polynomial function, $\varepsilon_r(T)$, which will then be used to compute the ε_r at each of the composite specimen data points. This method of generating an $\varepsilon_r(T)$ differs slightly from that used by Bowles. He fit his Moiré data from the reference grating test directly with a 3rd order least squares polynomial and then combined the coefficients of like terms from this polynomial with those of the 3rd order polynomial for the ULE, yielding a 3rd order polynomial for $\varepsilon_r(T)$. With the method described above, the choice of polynomial order to be used to fit the ε_r - T data is limited only by the number of the data points available.

3.4.5 Specimen Strains from Moiré Data

In the previous two sections procedures were given for reducing Moiré data to obtain the apparent strain, ε_m, and for determining the portion of this apparent strain, ε_r, attributable to changes in the reference grating. In order to translate these strains into the actual specimen strain, ε_s, a relationship linking ε_m, ε_r and ε_s must be developed. Recall

$$\varepsilon_m = -\frac{(N-N_i)}{L} \cdot g_r \tag{2.6}$$

$$g_r = 1/f_r \tag{2.4}$$

$$N = (f_r - \beta f_s) \cdot L \tag{3.1}$$

Substituting (3.1) and (2.4) into (2.6) and grouping reference and specimen frequencies:

$$\varepsilon_m = [(f_r - f_{r_i}) - \beta(f_s - f_{s_i})] \cdot \frac{1}{f_{r_i}} \tag{3.3}$$

Noting that, to within a very small fraction of a percent

$$\frac{\beta}{f_{r_i}} = \frac{1}{f_{s_i}}$$

Eqn. (3.3) may be rewritten

$$\varepsilon_m = \frac{f_r - f_{r_i}}{f_{r_i}} - \frac{f_s - f_{s_i}}{f_{s_i}} \tag{3.4}$$

Since strain is by definition change in length per original length,

then, in terms of frequencies, strain may be expressed

$$\varepsilon = \frac{f_1 - f}{f_1} \tag{3.5}$$

(Note: for positive strain, frequency decreases.) Substituting (3.5) into (3.4), and rearranging terms:

$$\varepsilon_s = \varepsilon_r + \varepsilon_m \tag{3.6}$$

which provides for the combination of any two known strains to determine the third. The computed strains and the temperatures to which they correspond are then fit with a least squares polynomial which can be differentiated with respect to temperature to yield the CTE.

4. EXPERIMENTAL ACCURACY

The experimental accuracy discussed here concerns only the ability to measure fringe orders and temperatures, and the effects of errors associated with these measurements on the quantitites determined from them. As noted earlier the displacement sensitivity of this technique is 833 nm (.33 μin.) per fringe. For the 33 mm (1.3 in.) gage length used in these tests this translates to a strain sensitivity of 25 με per fringe. The following analysis provides an estimate of the fractional fringe resolution capability as well as the overall error attributable to the data reduction process.

4.1 Fringe Orders and Apparent Strains

As indicated in Section 3.4.3 the change in fringe order at a gage mark from the initial test temperature to a subsequent temperature is the dependent variable in the least squares fit, and is referred to as ΔN.

The deviation of each ΔN_i from a first order curve was determined by comparing the ΔN_i with a $\Delta N(x_i)$ computed from the least squares slope and intercept, and x_i, the distance associated with the gage mark at which ΔN_i was measured. The average deviation of ΔN $\delta A_{\Delta N}$ - was computed from:

$$\delta A_{\Delta N} = \frac{\sum_{i=1}^{k} |\Delta N_i - \Delta N(x_i)|}{k} \qquad (4.1)$$

where k is the total number of data points used in all tests. For these tests which involved nearly 550 data points:

$$\delta A_{\Delta N} = 0.063 \text{ fringe} \tag{4.2}$$

As Beers [14] notes, the ratio of standard deviation to average deviation, for a large number of readings approaches 1.25. Using this factor and result (4.2) yields

$$S_{\Delta N} = 0.079 \text{ fringe} \tag{4.3}$$

Assuming that the fringe orders at each gage mark are read to the same accuracy, each of the two N's used to compute the ΔN_i would contribute the same random error to the ΔN_i. In light of Result (4.3) this assumption implies

$$S_n = 0.056 \text{ fringe} \tag{4.4}$$

This indicates the random error, to within one standard deviation, associated with reading a fringe order at a gage mark is approximately ±0.06 fringe.

Recalling Eqn. (3.2.b) and making use of (4.3) yields an overall standard deviation for the least square slope of

$$S_m = 2.15 \times 10^{-3} \text{ ℓ/mm} \tag{4.5}$$

Since the slope is multiplied by the pitch of the reference grating to obtain the apparent strain, ε_m, the standard deviation of the apparent strain is

$$S_{\varepsilon_m} = 1.8 \ \mu\varepsilon \tag{4.6}$$

4.2 Temperature

Determining the individual apparent strains, ε_m, and their accuray did not involve the temperature at which they occurred, but determining actual specimen strains as well as the CTE does involve the temperatures, and the accuracy to which the temperature is determined affects the accuracy of the specimen strains and predicted strains using the computed CTE. As stated at the end of Section 3.2.1 the temperature readouts were given to 0.1° F, and the thermocouples were read before and after each exposure. The overall standard deviation of the thermocouple readouts was found to be:

$$S_T = 0.25K \ (0.45\ ^0F) \qquad (4.7)$$

This temperature deviation must be included with the deviation in the strain to arrive at the expected error at a data point. To do this S_T must be expressed in terms of strain which is done by multiplying it by the slope of the ε - T curve, yielding a quanity $(S_T)_\varepsilon$. Even though the ε - T curves are non-linear, an average slope will be adequate for this conversion. This conversion will be illustrated in the following section.

4.3 Reference Grating and Composite Specimen

4.3.1 Reference Grating

As noted in Section 3.4.4 the quantities involved in determining ε_r at any data point in the prism calibration test are the computed ULE (specimen) strain and Moiré strain at that point. The deviation in the ULE ε - T curve is approximately 1 $\mu\varepsilon$ (see [3] Bowles), while the deviation in Moiré strain given by Eqn. (4.6) is 1.8 $\mu\varepsilon$. These combine to give:

$$S_{\varepsilon_r} = 2.0\ \mu\varepsilon \tag{4.8}$$

To determine the expected error in $\varepsilon_r(T)$, the contribution of temperature deviation must be added to Eqn. (4.8). The average slope of the $\varepsilon_r(T)$ (the function is given in the results section) is - 6.8 $\mu\varepsilon$/K.

This converts the temperature deviation given by Eqn. (4.7) to

$$(S_T)_\varepsilon = 1.7\ \mu\varepsilon \tag{4.9}$$

Values given by Eqns. (4.8) and (4.9) are combined to yield:

$$S_{\varepsilon_r}(T) = 2.7\ \mu\varepsilon \tag{4.10}$$

In evaluating the least square polynomial curve fits to the ε_r - T data the standard deviation of the 2nd order fit was found to be 2.3 $\mu\varepsilon$ which is within the expectations of Eqn. (4.10). However, a 3rd order fit produced a standard deviation of 1 $\mu\varepsilon$, and, although it is not felt

that this is an actual improvement in accuracy, this 3rd order polynomial was used to represent $\varepsilon_r(T)$.

4.3.2 Composite Specimen Strains

Since determining the strain in a composite specimen at any data point involves solving Eqn. (3.6), the errors expected in the strain include the combination of $S\varepsilon_r(T)$ and $S\varepsilon_m$. Recalling the results given in Eqns. (4.6) and (4.10) yield:

$$S\varepsilon_s = 3.2\ \mu\varepsilon \tag{4.11}$$

To evaluate the least squares fit to the specimen data the temperature deviation is converted to strain deviation as in the previous section and combined with Eqn. (4.11). The results for the composite laminates tested are given in Table 1.

Table 1

Expected Standard Deviation for Points on ε vs. T Curves

Laminate	$S_{\varepsilon_s}(T)$ ($\mu\varepsilon$)
[0]	3.2
$[0/\pm45/90]_s$	3.3
$[0/90/\pm45]_s$	3.3
[90]	7.6

5. RESULTS AND DISCUSSION

5.1 Reference Grating (Prism) Calibration

As noted in Section 3.4.4 the prism calibration was accomplished by running a thermal expansion test using ULE as the specimen and solving Eqn. (3.6) for ε_r, with the known ULE response for ε_s. The ULE response as determined by Bowles [3] is listed in Table 2. Equation (3.6) was solved for ε_r at each data point, and these points are shown in Fig. 9. A third order polynomial was generated as a least squares fit to these data points, and is also shown in Fig. 9, while its polynomial coefficients are listed in Table 2. Included in Fig. 9 is the third order least squares polynomial representation of the thermal response of Bowles' [3] reference grating. A comparison of the responses of the two reference gratings indicates the prism response to be ten times that of the reference grating used in [3], which leads to somewhat larger inaccuracies with the prism than with Bowles' diffraction grating. The greater thermal response of the prism causes an increased density of fringe patterns, making it sometimes more difficult and nearly always more laborious to evaluate the Moiré strain at a data point. This increased response also causes the error due to temperature inaccuracies to become significant even for laminates with a low thermal expansion coefficient. As noted in Section 3.2.3, follow up work with this technique will employ prisms having thermal response equivalent to or less than that of the reference grating used in [3].

Table 2

Polynomial Coefficients for Thermal Strain as a Function of Temperature

ε $\mu\varepsilon$	A_0 $\mu\varepsilon$ ($\mu\varepsilon$)	A_1 $\mu\varepsilon K^{-1}$ ($\mu\varepsilon^0 F^{-1}$)	A_2 $\mu\varepsilon K^{-2}$ ($\mu\varepsilon^0 F^{-2}$)	A_3 $\mu\varepsilon K^{-3}$ ($\mu\varepsilon^0 F^{-3}$)
ε_{ULE} (Bowles, et al.)	1.71424×10^2 (2.20232×10^0)	-1.38536×10^0 (-5.6844×10^{-2})	3.54245×10^{-3} (3.93171×10^{-4})	-2.76556×10^{-6} (-4.00045×10^{-7})
ε_r (Prism A-Reference Grating)	2.7835×10^3 (2.753×10^2)	-1.47121×10^1 (-3.7591×10^0)	2.62832×10^{-2} (1.49673×10^{-3})	-2.79936×10^{-5} (-4.8000×10^{-6})
ε_s [0] Laminate	2.8031×10^3 (5.805×10^1)	-2.2833×10^1 (-1.2007×10^0)	6.09685×10^{-2} (6.1811×10^{-3})	-5.34726×10^{-5} (-9.1687×10^{-6})
ε_s [90] Laminate	-4.1373×10^3 (-9.503×10^2)	3.5032×10^0 (1.19282×10^1	3.52007×10^{-2} ($1.08641 \times$ $^{-2}$	—
ε_s $[0/\pm45/90]_s$ Laminate	-1.058×10^2 (-7.40×10^1)	-1.2323×10^0 (8.23169×10^{-1})	5.3170×10^{-3} (1.6410×10^{-3})	—
ε_s $[0/90/\pm45]_s$ Laminate	-7.33×10^1 (-6.172×10^1)	-1.2174×10^0 (7.2650×10^{-1})	4.9468×10^{-3} (1.5268×10^{-3})	—

$$\varepsilon = A_0 + A_1 T\ A_2 T^2 + A_3 T^3$$

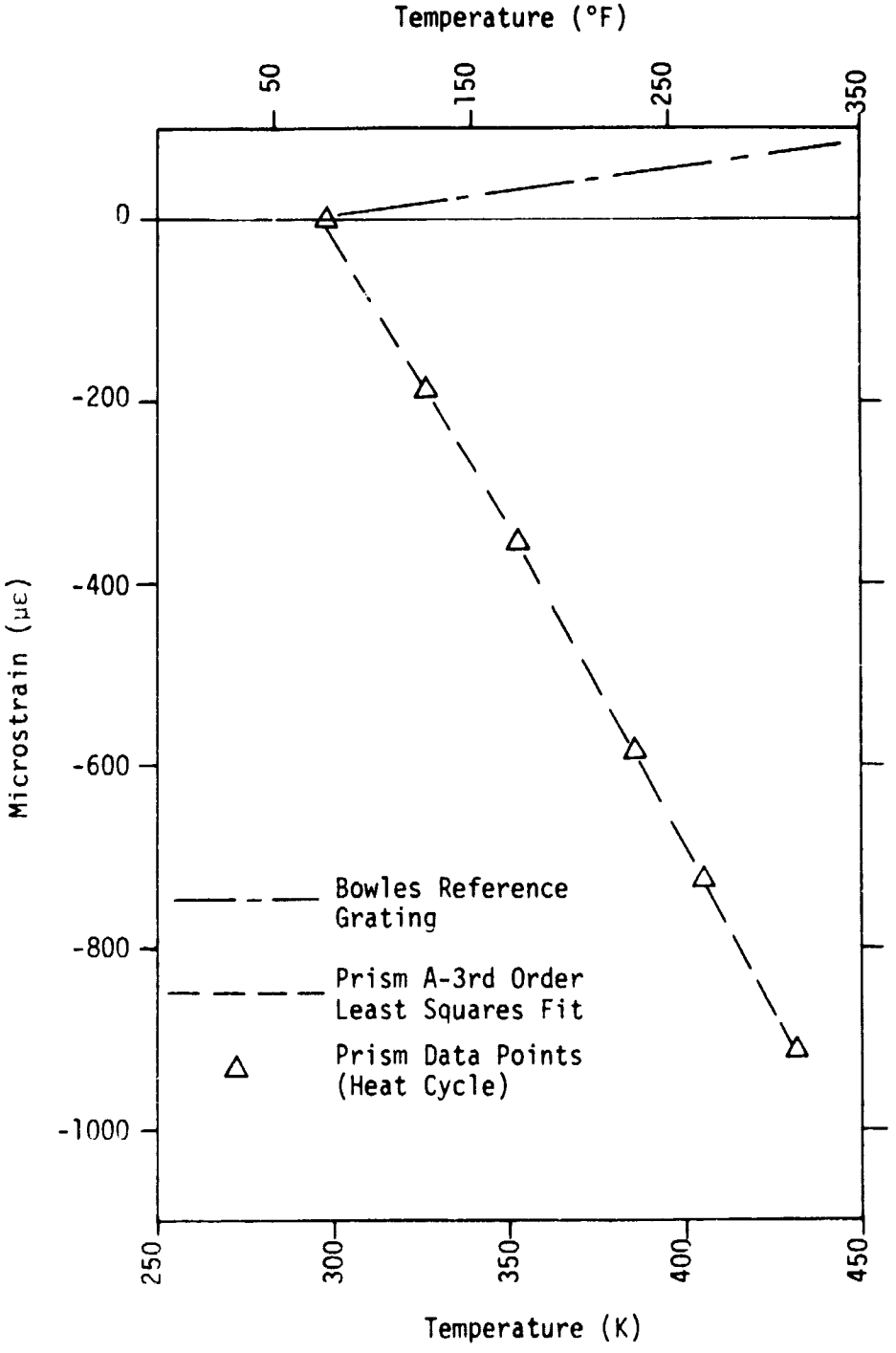

Fig. 9 Thermal Expansion of Reference Grating (Prism A)

In the test program for the prism calibration, there were two deficiencies which have made confident evaluation of the results less than optimum. First, data was only taken at points on the heating cycle, and although the response of the prism should be the same on heat up and cool down, factors in the system such as movement of a prism in the prism-holding frame over a complete cycle and the correctness of the thermocouples in measuring the temperature of both the specimen and the prisms for a heating and cooling condition were not evaluated. Second, only one prism was calibrated since, as was mentioned in Section 3.4.4, a prism-holding frame was needed as the support for the ULE specimen. For small thermal responses, variations which might occur in prisms cut from the same glass would not become significant. But for thermal responses much larger than those of the specimen being measured, small variations in the prisms may produce a significant error in the test results. In addition, movement of prisms in the holding frames may not be the same for both prisms, although it is probably repeatable cycle to cycle. These two possible sources of error in the prism calibration, and hence all other test results, can be removed by making a third holding frame and testing each prism through at least two complete heat up and cool down cycles.

5.2 Thermal Expansion of Composite Laminates

The results for the composite test specimens are grouped by laminate type. Unless otherwise noted, all strains presented in this section

are the average of the strains computed for each side of the laminate. Tables 3 and 4 present numerical results (from best fit polynomials) of strain and CTE at selected temperatures for all laminates and a numerical comparison with Bowles results.

As noted in Section 3.3 the laminates were dried at 340 K (150°F) in an oven without an enforced dry atmosphere. As a consequence of this, it is felt that at test temperatures above the drying temperature additional moisture desorbtion took place. This desorbtion would cause varying amounts of contraction (depending on laminate type) during the heating cycle, which, due to slower absorbtion than desorbtion rates, would not necessarily be recovered during the cooling cycle. The effect on the strain vs. temperature response would be lower strains during the cooling cycle than those measured at corresponding temperatures during the heating cycle. This effect was observed, to some extent, for all composite laminates tested, which in a qualitative sense provides some verification for the existence of the desorbtion discussed above.

5.2.1 [0] Laminate

The strain vs. temperature results for the [0] laminate are shown graphically in Fig. 10. A 3rd order least squares fit of the data was used, with the polynomial coefficients given in Table 2. The standard deviation of the data points from this curve fit is $2\mu\varepsilon$. Bowles' best fit curve is shown for comparison. As noted in Section 3.1, steps taken to improve the alignment of gage markes on grating molds and grating

Table 3

Thermal Strain Comparison - Brooks/Bowles[2]

Laminate (Specimen Designation)	$\varepsilon(\mu\varepsilon)$ Brooks/Bowles [2] (From Best Fit Curves)		
	297 K (75° F)	360 K (189° F)	422 K (300° F)
[0] (38-21 B)	-2.6/0	-10.7/-6.7	16.2/-13.4
[90] (39-30 A)	10/25	1685/1583	3610/3425
$[0/\pm45/90]_S$ (43-7)	-3/4	140/139	321/302
$[0/90/\pm45]_S$ (44-8 B)	2/-2	130/138	294/297

Table 4

CTE for T300/5208 Laminates

Laminate	CTE $\mu\varepsilon K^{-1}$ ($\mu\varepsilon°F^{-1}$)					
	297K (75°F)		360K (189°F)		422K (300°F)	
	Brooks	Bowles[2]	Brooks	Bowles[2]	Brocks	Bowles[2]
[0]	-0.768 (-0.427)	-0.107 (-0.059)	0.274 (0.152)	-0.107 (-0.059)	0.057 (0.032)	-0.107 (-0.059)
[90]	24.42 (13.56)	22.23 (12.35)	28.85 (16.03)	27.24 (15.13)	33.21 (18.45)	32.18 (17.88)
$[0/\pm45/90]_s$	1.93 (1.07)	1.89 (1.05)	2.60 (1.44)	2.38 (1.32)	3.25 (1.81)	2.87 (1.59)
$[0/90/\pm45]_s$	1.75 (0.97)	2.05 (1.14)	2.06 (1.44)	2.40 (1.33)	2.96 (1.64)	2.73 (1.52)

molds on the specimen eliminate the need to apply the rotational correction factors given by Bowles. A comparison between Figs. 9 and 10 indicates the extent to which the [0] laminate Moiré results were dominated by the apparent strain of the reference gratings. This is not a desirable situation and as was indicated in Section 3.2.3 this difficulty will be corrected in follow up work. Although the general shape of the ε vs. T curve generated from this test, i.e. compressive strains with heating up to approximately 330 to 340 K (135 to 150°F), and tensile strains from that point up to the temperature limit of this test, differs from Bowles' Moiré results of linear, compressive ε vs. T, qualitatively, these results are in agreement with Bowles' strain gage results [3], and are very similar to strain gage results obtained by Hyer and Hagaman [15] on Graphite-Polyimide material systems.

Fig. 11 presents the ε(W/Bending) vs. T data points. These points are delineated as Side 1 or Side 2 and whether they occurred during a heating or cooling cycle. The bending strains derived by comparison of Side 1 and Side 2 data (1 to 10 $\mu\varepsilon$) could be an indication of nonuniformity in the fiber distribution or curing process, but unfortunately as noted in section 5.1, it is conceivable that side to side variations of this amount could also be due to variations in the response of the two prisms used here. Hopefully this question will be resolved in follow-up tests. Figure 11 also indicates generally higher strains (0 to 6 $\mu\varepsilon$) during heating cycles than cooling cycles. It is not likely that this could be attributed to the moisture desorbtion

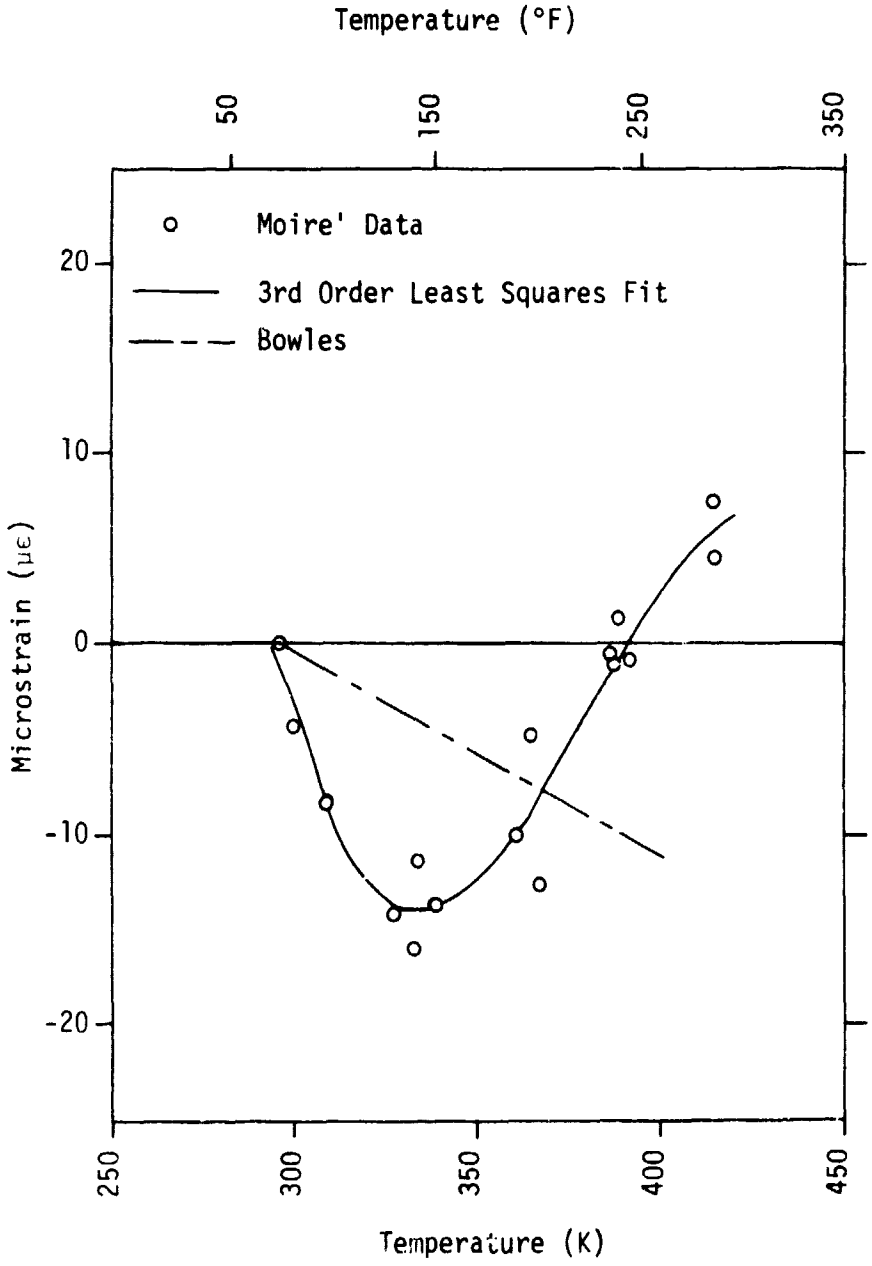

Fig. 10 Thermal Expansion - [0] Laminate

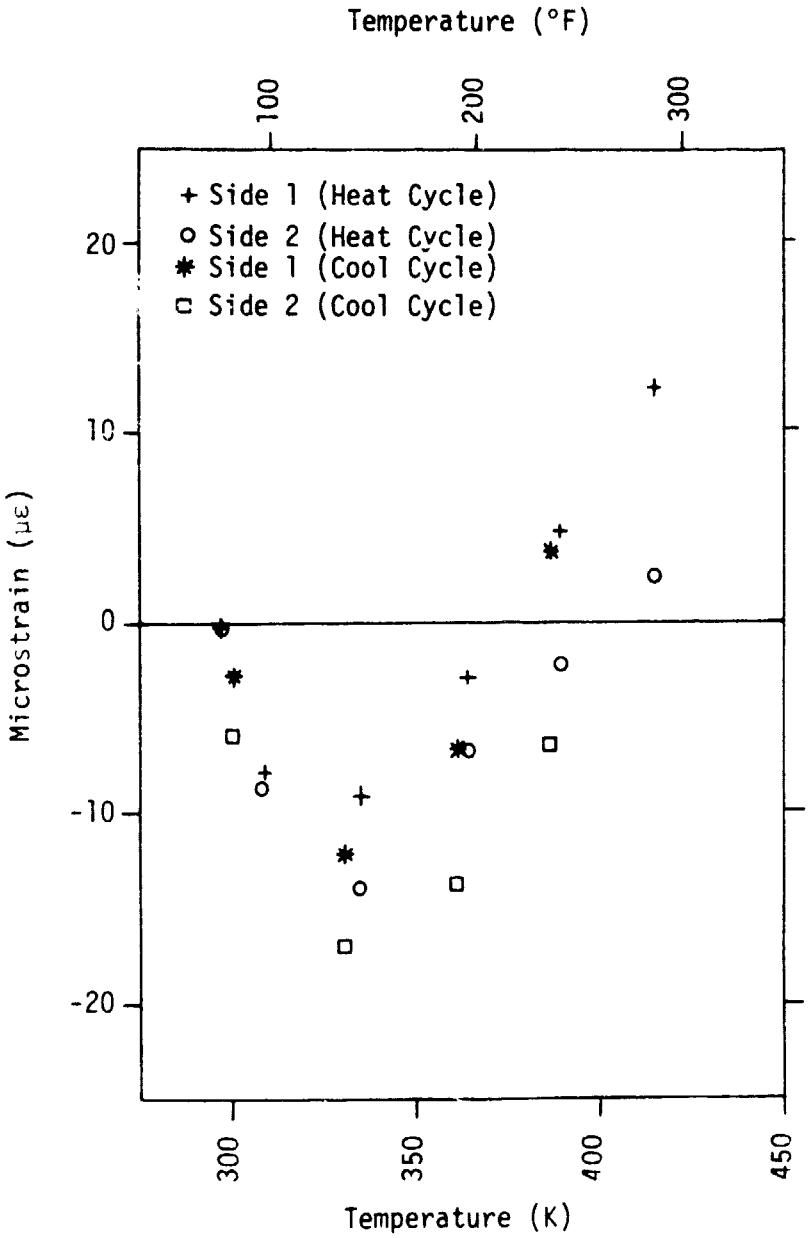

Fig. 11 ε (W/Bending) Vs. T [0] Laminate

problem noted in Section 5.2, since the [0] laminate is not sensitive to moisture desorbtion in this temperature range. The most likely source for this consistent discrepancy in heating and cooling cycles for the [0] laminate is in differing prism response (either mechanical or material) during heating and cooling which, as noted in Section 5.1, was not measured prior to testing.

5.2.2 [90] Laminate

Fig. 12 presents the strain vs. temperature results for the [90] laminate. A second order least squares fit of the data was used, with the polynomial coefficients given in Table 2. The standard deviation of the data points from this curve fit is 8.8 $\mu\varepsilon$ which is close to the expected standard deviation of 7.6 $\mu\varepsilon$ given in Table 1. Using the data for the heating cycle only results in a deviation of only 3$\mu\varepsilon$. The data points on the cooling cycle had lower strains than points on the heating cycle at comparable temperatures with a maximum difference of approximately 35$\mu\varepsilon$ at 310 K (100°F) - the lowest temperature on the cool down cycle. As indicated in Section 5.2 this could possibly be the result of continued desorbtion. Using the lamina coefficients of moisture expansion (CME) reported by Hahn and Kim [16],

$$\beta_1 = 0 \text{ and } \beta_2 = 5900\ \mu\varepsilon/\%\ H_2O$$

the 35 $\mu\varepsilon$ difference noted between the heating and cooling cycles of the

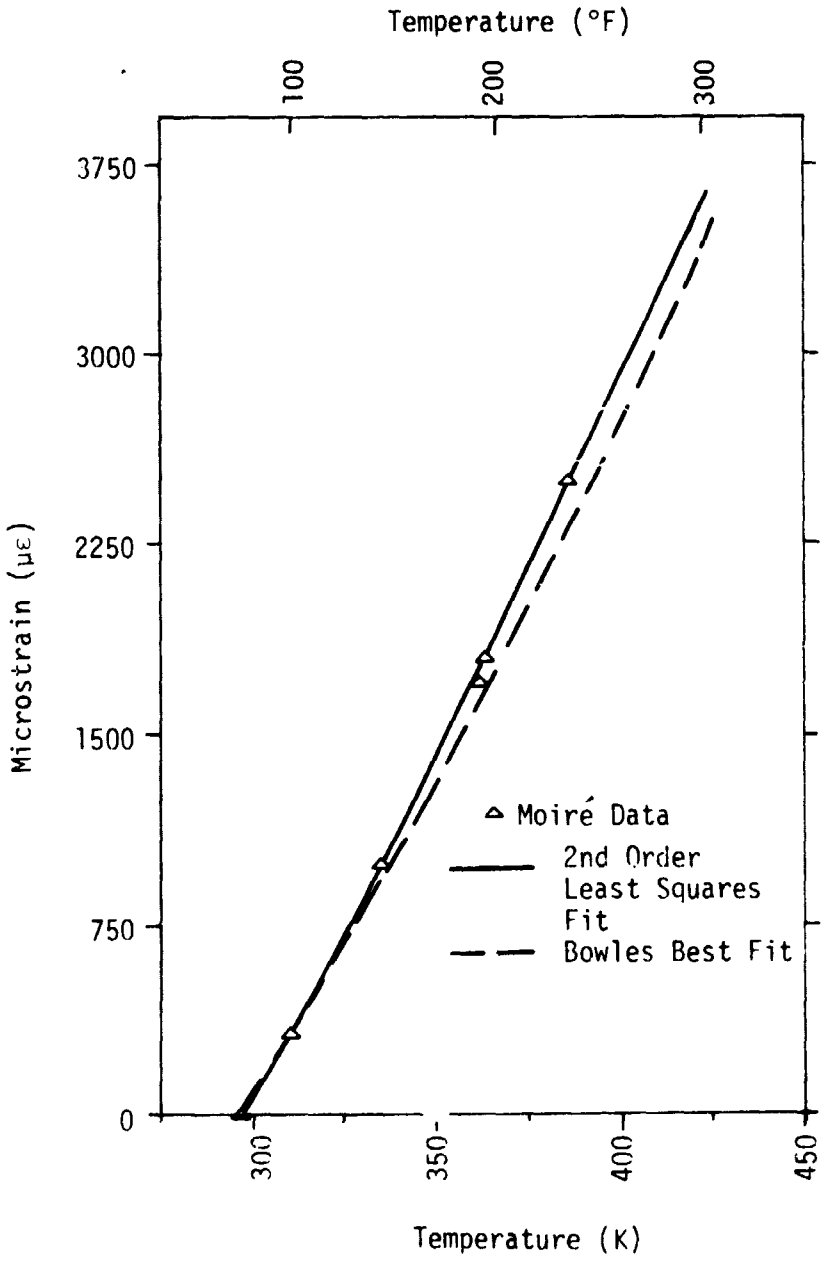

Fig. 12 Thermal Expansion - [90] Laminate

[90] laminate would require an additional moisture loss of 0.007% during testing. This does not seem unreasonable given the environmental conditioning prior to testing. The strains obtained in these tests were approximately 7% higher than those obtained by Bowles. After the initial temperature increment there was a fairly constant difference in strain from Side 1 to Side 2 of 25 - 30 $\mu\varepsilon$. A constant difference would not indicate bending, but since one side could not be considered more correct than the other, they were averaged just as the other results were.

5.2.3 $[0/+45/-45/90]_S$ Laminate

Fig. 13 presents the strain vs. temperature results for the $[0/+45/-45/90]_S$ laminate. A second order least squares fit of the data was used, with the polynomial coefficients given in Table 2. The standard deviation of the data ponts from this curve fit is 7.8 $\mu\varepsilon$ which is more than double the expected deviation given in Table 1. The problem is not likely to be in the appropriateness of the order of curve fit chosen, as a second order fit has been sufficient in most other laminates, and a third order fit offered only slight improvement (standard deviation of 7.1 $\mu\varepsilon$). The heating cycle itself had (for a second order fit) a deviation of 5 $\mu\varepsilon$ which is worse than the anticipated deviation and indicates the presence of an erroneous data point. Moreover, the cooling cycle strains are 15-20 $\mu\varepsilon$ below those expected from the fit of the heating cycle data points causing the even larger deviation when all

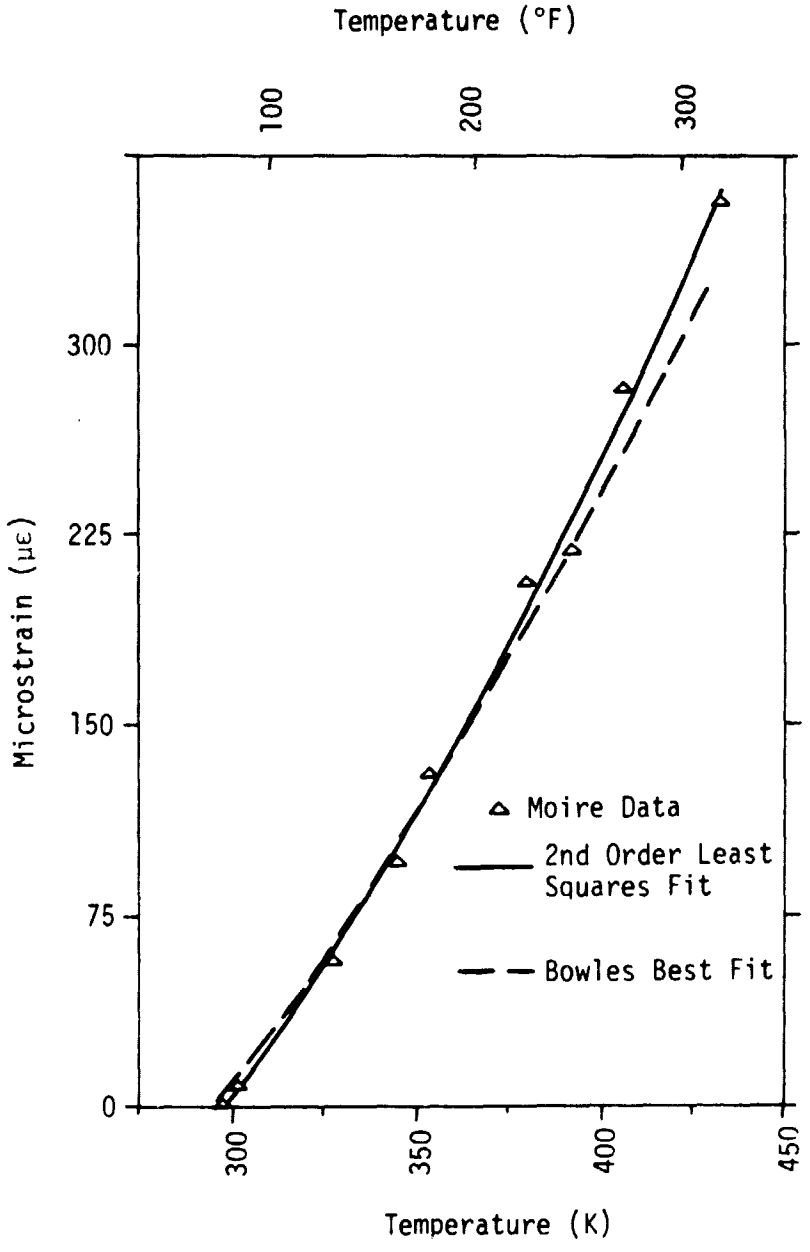

Fig. 13 Thermal Expansion - $[0/+45/-45/90]_s$ Laminate

points are used in the curve fitting process. Again, this heating and cooling cycle difference is thought to be primarily attributable to moisture desorbtion during testing. Using laminate analysis, the CME's noted in the previous section, and the elastic properties given in Table 5, the laminate CME for the quasi-isotropic laminates is found to be

$$\beta_{\text{quasi-isotropic}} = 514\ \mu\varepsilon/\%\ H_2O$$

For the strains noted this implies additional moisture desorbtion during testing of 0.03 to 0.04% of the composites weight. Even though these moisture losses are higher than those noted for the [90] laminate, they still seem to be within reason.

Table 3 indicates these strains to range from 0 - 6% higher than those obtained by Bowles, with a larger discrepancy for CTE found in Table 4. Side 1 and Side 2 strains differed by at most 6 $\mu\varepsilon$, indicating very little bending during testing.

5.2.4 $[0/90/+45/-45]_S$ Laminate

Fig. 14 presents the strain vs. temperature for the $[0/90/+45/-45]_S$ laminate. A second order least squares fit of the data was used, with the polynomial coefficients given in Table 2. The standard deviation of the data points from this curve fit is 4.8 $\mu\varepsilon$, which is approximately 50% higher than the expected deviation given in Table 1. For the heating cycle data points a second order fit yielded a deviation of only 2 $\mu\varepsilon$, with the cooling data points about 5 - 10 $\mu\varepsilon$ less than expected

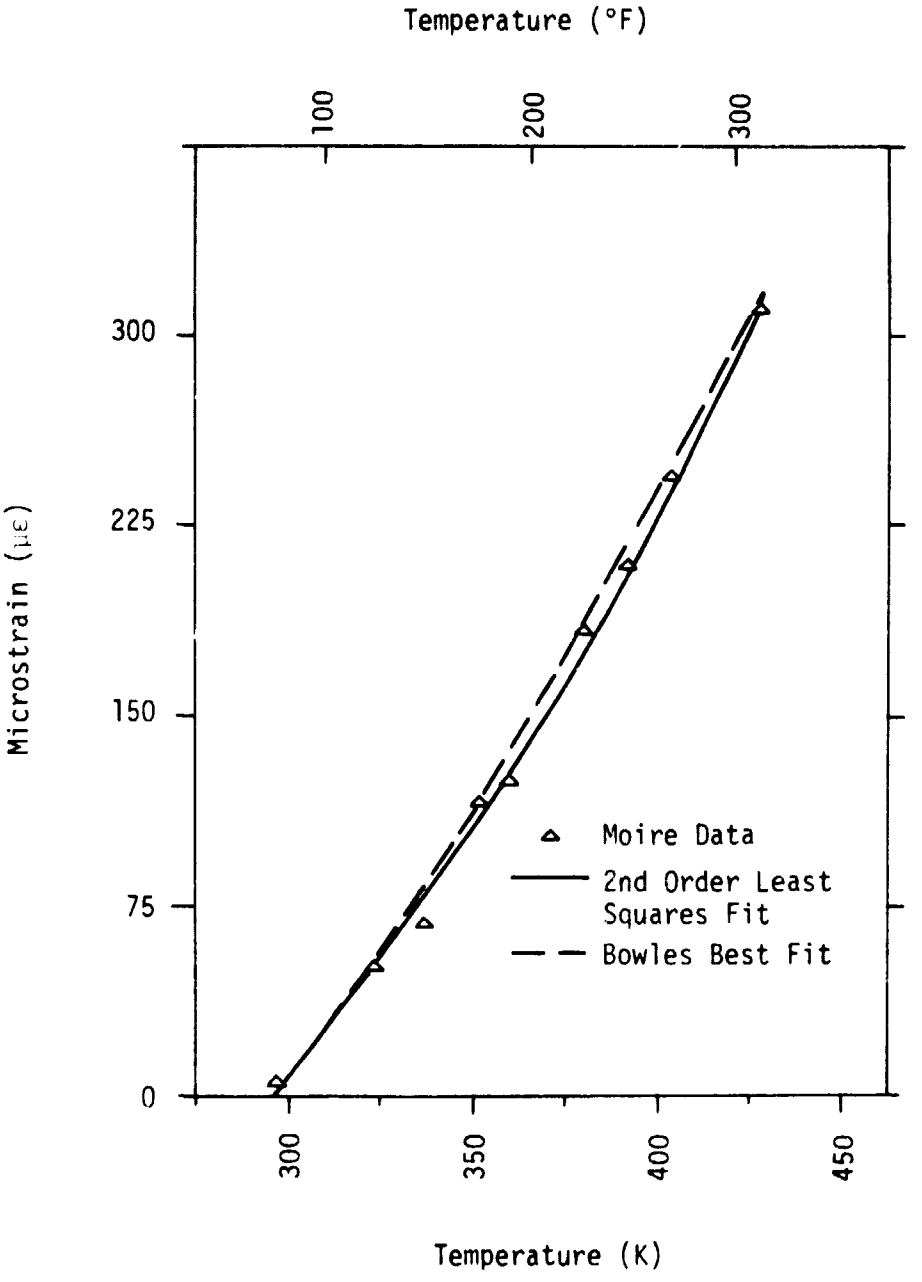

Fig. 14 Thermal Expansion - $[0/90/+45/-45]_s$ Laminate

from the heating cycle curve fit. Again this indicates the possibility of moisture desorbtion during testing. Using the CME generated in the previous seciton, these strains could result from moisture desorbtion of 0.01 to 0.02% of the composites weight, which as noted in the previous section is a reasonable possibility.

As Tables 3 and 4 indicate results for this laminate are in better agreement with Bowles' results, possibly because this laminate was the closest to exhibiting "dry" behavior. The Side 1 to Side 2 strain difference varied almost linearly from 0 $\mu\varepsilon$ at room temperature to 32 $\mu\varepsilon$ at 428 K (311°F). Bending strains of this magnitude are not surprising in nominally symmetric quasi-isotropic laminates, especially considering the surface preparation method prior to grating application noted in Section 3.3. It would also seem that since Bowles had to prepare only one surface of his quasi-isotropic specimens the danger of creating a slightly anti-symmetric laminate resulting in slight bending would be even greater. Fig. 15 presents an interesting possibility concerning bending and comparison of Bowles' results with those obtained in these tests. Side 1 and Side 2 data are plotted individually along with Bowles' best fit curve. For the most part the best fit curve lies between the data from Side 1 and Side 2, and in very close agreement with Side 1 data.

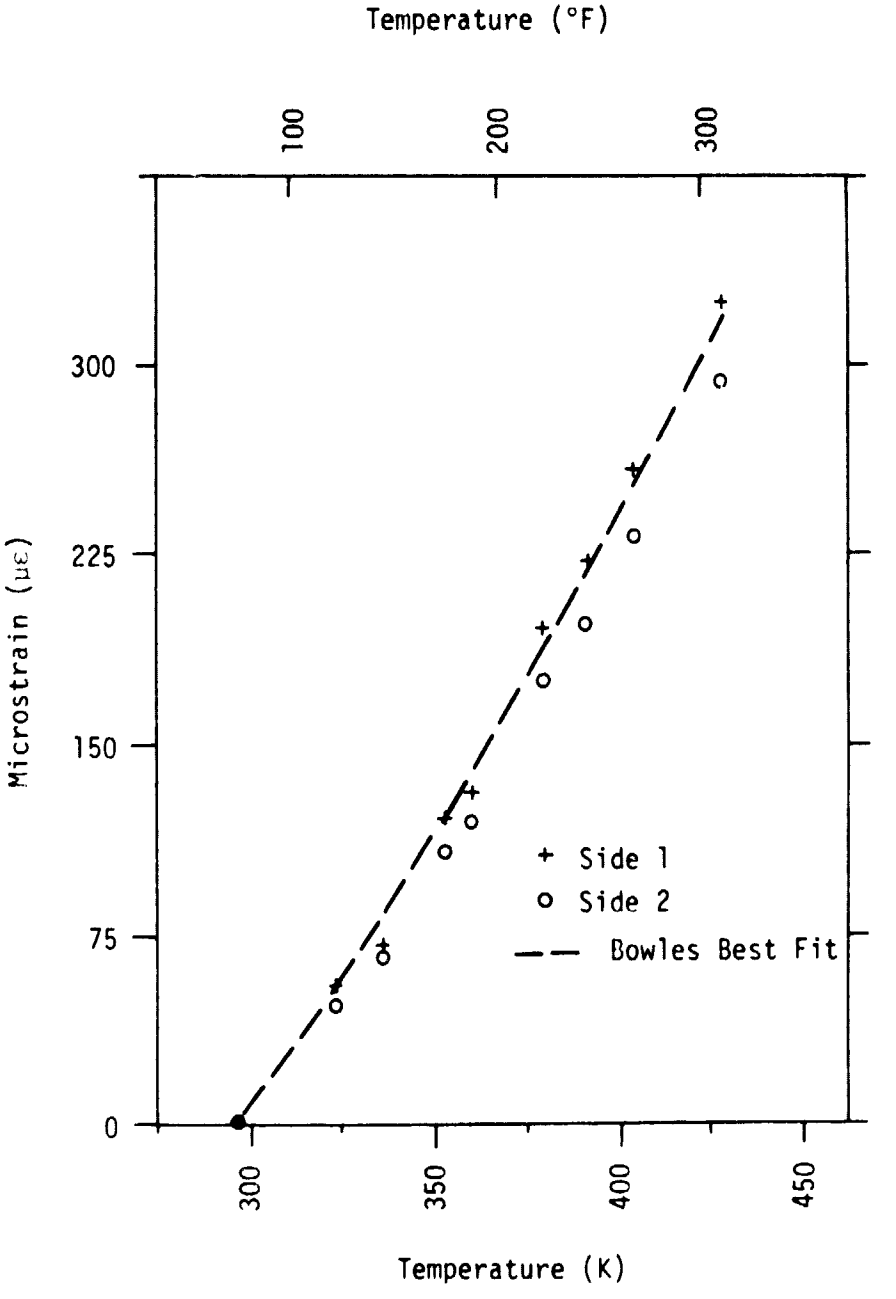

Fig. 15 ε (W/Bending) Vs. T - $[0/90/+45/-45]_s$ Laminate

5.3 Comparison with Lamination Theory

A macromechanics approach based on the method of classical laminated plate theory will be used to predict the thermoelastic response of the two quasi-isotropic laminates tested here. The method uses the thermoelastic behavior of the individual laminae in conjunction with the orientation and thickness of each lamina to predict the behavior of the laminate. The lamina thermal properties were based on the results obtained in the [0] and [90] laminate tests, which may be found in Table 2. The lamina elastic properties are those used by Kriz, et al. [17] for T300/5208 in the dry state. These properties are given in Table 5. Since the elastic properties are assumed independent of temperature, the analysis presented here will have temperature dependence only for the thermal properties. The lamination theory used here follows the analysis presented by Hahn and Pagano [18]. In particular, for symmetric laminates they show

$$\{\varepsilon^0(T)\} = [A'] \{N^T(T)\} \tag{5.1}$$

where $\{\varepsilon^0(T)\}$ is the temperature dependent midplane strain of the laminate, $[A']$ is the inverse of the extensional stiffness matrix and $\{N^T(T)\}$ is the temperature dependent thermal force resultant which may be expressed

$$\{N^T(T)\} = \int_{-H}^{H} [\bar{Q}]^K \{\varepsilon^T(T)\}^K dz \tag{5.2}$$

TABLE 5
ELASTIC PROPERTIES FOR T300/5208

Elastic Property	Lamina Value GPa (MSI)
E_1	130.3 (18.9)
E_2	9.72 (1.41)
G_{12}	5.39 (.782)
ν_{12}	0.308

where $[\bar{Q}]^K$ are the transformed stiffnesses of the Kth layer and $\{\varepsilon^T(T)\}^K$ is the temperature-dependent free thermal strain of the Kth layer. Assuming all plies to have the same thickness, t, Eqn. 5.2 may be simplified and substituted into Eqn. 5.1 to yield

$$\{\varepsilon^0(T)\} = 2t\,[A']\sum_{K=1}^{N}[\bar{Q}]^K\,\{\varepsilon^T(T)\}^K \tag{5.3}$$

where N is one-half the number of plies in a symmetric laminate. Since stacking sequence has no effect in symmetric laminates under uniform thermal loading, Eqn. 5.3 may be solved for the $[0/+45/-45/90]_s$ laminate configuration, with results that would apply equally to the $[0/90/+45/-45]_s$ configuration. This solution is presented in Fig. 16 along with moiré data points from the two quasi-isotropic laminates tested. Comparison is exceptionally good for the $[0/+45/-45/90]_s$ laminate and fairly good for the $[0/90/+45/-45]_s$ laminate.

By definition the CTE $\{\alpha(T)\}$ is given by:

$$\{\alpha(T)\} = \frac{d}{dT}\{\varepsilon^0(T)\} \tag{5.4}$$

which is solved for $\alpha_x(T)$ at several temperatures for the quasi-isotropic laminate configurations used here. Results are presented on these laminates in Table 6. Again, agreement is reasonably good.

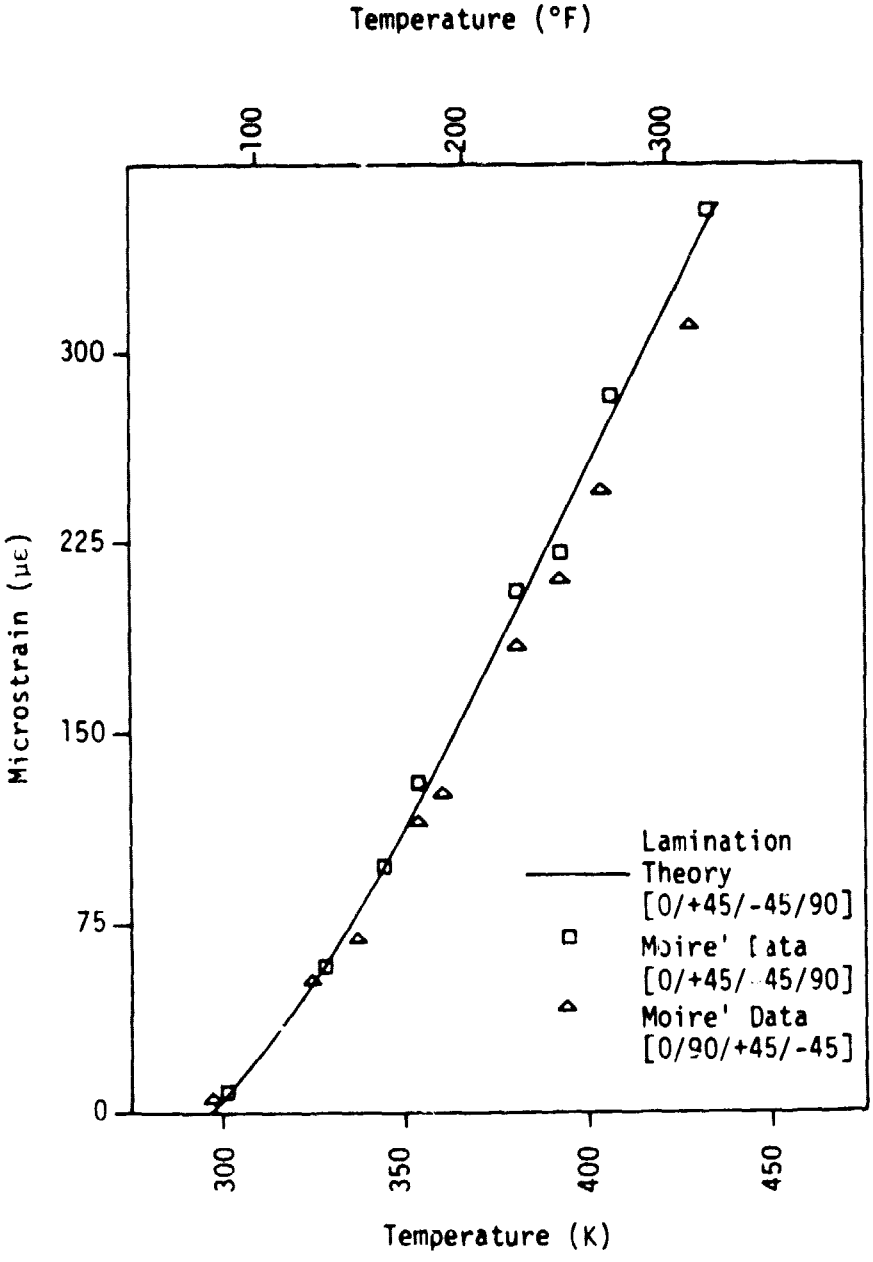

Fig. 16 Comparison of Lamination Theory With Moire' Data

TABLE 6

LAMINATION THEORY CTE AND COMPARISON
WITH TEST RESULTS

T (K/°F)	CTE (Theoretical) ($\mu\varepsilon K^{-1}/\mu\varepsilon °F^{-1}$)	CTE (Experimental) ($\mu\varepsilon K^{-1}/\mu\varepsilon °F^{-1}$)	
	$[0/+45/-45/90]_S$ and $[0/90/+45/-45]_S$	$[0/+45/-45/90]_S$	$[0/90/+45/-45]_S$
297/75	1.42/0.79	1.93/1.07	1.72/0.96
328/131	2.23/1.24	2.25/1.25	2.03/1.13
360/189	2.76/1.53	2.60/1.44	2.34/1.30
391/244	2.99/1.66	2.93/1.63	2.65/1.47
422/300	2.94/1.63	3.26/1.81	2.96/1.64

6. CONCLUSIONS

The primary purpose of this investigation was to develop an experimental technique for using moiré interferometry to measure the thermal response of both sides of composite laminate coupon specimen. In conjunction with this, it was desired that the technique developed be easily extended to temperature regimes not encountered in this and previous tests using moiré interferometry. To accomplish these goals partially mirrorized glass prisms were employed to generate virtual diffraction gratings in an experimental setup designed for simultaneous viewing of both sides of the laminate being tested. Improvements were made in the methods for marking gage lines on the grating molds and aligning these molds on the specimen. The number of data points needed was reduced by 40% from the number used by Bowles [3]. The thermal response of the laminates determined here was compared with that given by Bowles [3] and with lamination theory. Results here led to the following conclusions:

1) Moiré interferometry, with partially mirrorized prisms used to form virtual reference gratings in a changing thermal environment, has been determined to be an effective and potentially precise technique for the experimental determination of the thermal response of lamianted composites in a temperature range of 297 K (75°F) to 422 K (300 °F). Fringe patterns generated with this technique were sharp and had excellent contrast.
2) Simultaneous two-sided viewing has been shown to provide useful information on side-to-side, non-uniform behavior. For the

quasi-isotropic lamiantes tested, these side-to-side variations were found to be as much as 10% of the longitudinal strains.

3) The CTE's of the four T300/5208 graphite-epoxy laminates, as determined by this investigation, are summarized as follows: the [0] laminate has a quadratic temperature dependent CTE ranging from -0.768 $\mu\varepsilon K^{-1}$ @ 297 K (75°F) thru a value of 0.00 @ 334K (142 °F) to a relative maximum of 0.34 $\mu\varepsilon K^{-1}$ @ 380 K (255 °F) and ending with a value of 0.057 $\mu\varepsilon K^{-1}$ @ 422 K (300 °F); the [90] laminate has a linear temperature dependent CTE ranging from 24.41 $\mu\varepsilon K^{-1}$ @ 297 K (75 °F) to 33.21 $\mu\varepsilon K^{-1}$ @ 422 K (300 °F); the $[0/+45/-45/90]_S$ laminate has a linear temperature dependent CTE ranging from 1.93 $\mu\varepsilon K^{-1}$ @ 297 K (75 °F) to 3.25 $\mu\varepsilon K^{-1}$ @ 422 K (300 °F); the $[0/90/+45/-45]_S$ laminate has a linear temperature dependent CTE ranging from 1.72 $\mu\varepsilon K^{-1}$ @ 297 K (75 °F) to 2.96 $\mu\varepsilon K^{-1}$ @ 422 K (300 °F). These two quasi-isotropic laminates have identical CTE's of 2.60 $\mu\varepsilon K^{-1}$ @ the test's mid-point temperature of 360 K (189 °F).

4) Comparison with Bowles showed generally good agreement between the two Moiré techniques, with differences in thermal response on the order of less than 7% in the [90] and two quasi-isotropic lamiantes. The [0] laminate had a completely different shape to its thermal response curve than that found by Bowles using Moiré interferometry, but had a similar shape to that found by Bowles using strain gages as well as that found by Hyer and Hagaman using strain gages on graphite polyimide. The comparison with lamination

theory yielded for the most part better than 5% agreement between actual and theoretically predicted strains for the quasi-isotropic laminates.

5) The effect of residual moisture in laminates with some environmental conditioning appears to be significant. After driving out approximately 0.4-0.5% of the laminate's weight in moisture prior to testing, response typical of continued moisture desorption was observed during testing. Strains of as much as 35 με were attributed to this type of response.

The basic test method developed appears to be sound and worth continuing with modifications as noted elsewhere in this report and summarized here:

1) New prisms using glass with a much smaller change in index of refraction with temperature;
2) Calibration of both prisms through several heating and cooling cycles to remove any question about their contribution to the results;
3) Specimens must be dried and tested in an oven with an enforced dry atmosphere.

REFERENCES

1. Wolff,E. G., "Measurement Techniques for Low Expansion Materials,"Materials and Processes - In Service Performance, Vol. 9, National SAMPE Technical Conference, October 1977.

2. Bowles, D. E., D. Post, C. T. Herakovich, and D. R. Tenney, "Moiré Interferometry for Thermal Expansion of Composites," Experimental Mechanics, Vol 21, No. 12, Dec. 1981, pp. 441-447.

3. Bowles, D. E., D. Post, C. T. Herakovich, and D. R. Tenney, "Thermal Expansion of Composites Using Moire Interferometry," VPI-E-80-19, Virginia Polytechnic Institute and State University, Blacksburg, Virginia, July 1980.

4. Eselun, S. A., H. D. Neubert and E. G. Wolff, "Microcracking Effects on Dimensional Stability," 24th National SAMPE Symposium and Exhibition, 1979.

5. Reifsnider, K. L., and J. E. Masters, "Investigation of Characteristics Damage States in Composite Laminates," Proceedings, ASME Annual Meeting, San Francisco, Calif., Dec. 1978.

6. Herakovich, C. T., J. G. Davis, Jr., and J. S. Mills, "Thermal Microcracking in Celion/PMR-15 Graphite/Polyimide," Thermal Stresses in Severe Thermal Environments, (Hasselman and Heller, editor). New York: Plenum Publishing Corp., 1980.

7. Guild, J., The Interference Systems of Crosses Diffraction Gratings. Oxford: Claredon Press, 1956.

8. Chiang, Fu-Pen, "Moiré Methods of Strain Analysis," Manual on Experimental Stress Analysis, 3rd ed. Society for Experimental Analysis.

9. Post, D., "Optical Interference for Deformation Measurements - Classical Holographic and Moiré Interferometry," Mechanics of Nondestructive Testing, (W. W. Stinchcomb, ed.). New York: Plenum Publishing Corp., 1980.

10. Post, D., "Moiré Fringe Multiplication with a Non-Symmetrical Doubly Blazed Reference Grating," Applied Optics, Vol. 10, No. 4, April 1971, pp. 901-907.

11. Walker, C. A. and J. McKelvie, "A Practical Multiplied Moiré System, Experimental Mechanics, Vol. 18, No. 8, August 1978, pp. 316-320.

12. Rowlands, R. E. and J. H. Vallem, "On Replication for Moiré Fringe Multiplication, Fringe Mechanics, Vol. 20, No. 5, May 1980, pp. 167-169.

13. Post, D. and W. A. Baracat, "High Sensitivity Moiré Interferometry - A Simplified Approach," Experimental Mechanics, Vol. 21, No. 3, March 1981, pp. 100-104.

14. Beers, Yardley, Introduction to the Theory of Error, Addison-Wesley Publishing Company, Inc.

15. Hyer, M. W. and Hagaman, J. A., "Thermal Cycling of Graphite Polyimide," VPI-E-79-15, Virginia Polytechnic Institute and State University, Blacksburg, Virginia, April 1979.

16. Hahn, H. T. and Kim, R. Y., "Swelling of Composite Laminates," Advanced Composite Materials - Environmental Effects, ASTM 658, American Society for Testing Materials, 1978, pp. 98-120.

17. Kriz, R. D., Stinchcomb, W. W., Tenney, D. R., "Effects of Moisture, Residual Thermal Curing Stresses and Mechanical Load on the Damage Development in Quasi-Isotropic Laminates," Virginia Polytechnic Institute and State University, VPI-E-80-5, 1980.

18. Hahn, H. T. and N. J. Pagano, "Curing Stresses in Composite Laminates," J. Comp. Materials, Vol. 9 (Jan. 1975), pp. 91-106.